CrossMark

J. Fluid Mech. (2017), *vol.* 832, *pp.* 345–382. © Cambridge University Press 2017
doi:10.1017/jfm.2017.642

Continuum theory for rapid cohesive-particle flows: general balance equations and discrete-element-method-based closure of cohesion-specific quantities

Kevin M. Kellogg[1], Peiyuan Liu[1], Casey Q. LaMarche[1] and Christine M. Hrenya[1,†]

[1]Department of Chemical and Biological Engineering, University of Colorado at Boulder, Boulder, CO 80309, USA

(Received 17 January 2017; revised 6 September 2017; accepted 7 September 2017; first published online 26 October 2017)

The continuum description of rapid cohesive-particle flows comprises the population balance, which tracks various agglomerate sizes in space and time, and kinetic-theory-based balances for momentum and granular energy. Here, fundamental closures are provided in their most general form. In previous population balances, the probability ('success factor') that a given collision results in agglomeration or breakage has been set to a constant even though it is well established that the outcome of a collision depends on the impact (relative) velocity. Here, physically based closures that relate the success factors to the granular temperature, a (continuum) measure of the impact velocity, are derived. A key aspect of this derivation is the recognition that the normal component of the impact velocity dictates whether agglomeration occurs. With regard to the kinetic-theory balances, cohesion between particles makes the collisions more dissipative, thereby decreasing the granular temperature. The extra dissipation due to cohesion is accounted for using an effective coefficient of restitution, again determined using the derived distribution of normal impact velocities. This collective treatment of the population and kinetic-theory balances results in a general set of equations that contain several parameters (e.g. critical velocities of agglomeration) that are cohesion-specific (van der Waals, liquid bridging, etc.). The determination of these cohesion-specific quantities using simple discrete element method simulations, as well as validation of the resulting theory, is also presented.

Key words: granular media, multiphase flow, particle/fluid flow

1. Introduction

Cohesion between solid particles may stem from van der Waals forces and liquid bridging, to name a few possibilities (Visser 1989; Henthorne & Hrenya 2012; Galvin & Benyahia 2014). When the cohesive force acting on a particle is comparable to other forces acting on the particle (e.g. the weight of the particle), particles may

† Email address for correspondence: hrenya@colorado.edu

https://doi.org/10.1017/jfm.2017.642 Published online by Cambridge University Press

aggregate together to form clusters of particles called agglomerates (Castellanos 2005). Aggregation can have dramatic effects on flows of particles, such as decreasing the entrainment of particles in a fluidized bed (Geldart, Harnby & Wong 1984), affecting the segregation and mixing of particles (Tomas 2004) and many more (Tomas 2004; Calvert, Ghadiri & Tweedie 2009; Galvin & Benyahia 2014). Empirical predictions for the entrainment rate and transport disengagement height of particles in a fluidized bed vary by many orders of magnitude (Cahyadi *et al.* 2015; Chew *et al.* 2015), even before taking cohesion into account (Motlagh *et al.* 2014). A better physical understanding of aggregation and its effects is needed. Here, the focus is on the first-principles prediction of cohesive solids engaged in 'rapid' flows, i.e. dilute to moderately dense flows in which the contacts are approximately binary and instantaneous in nature, rather than the enduring and multi-contact nature of very dense flows.

The discrete element method (DEM) is one approach available for the prediction of aggregation in rapid cohesive-powder flows. In the DEM, particles are tracked individually using Newton's second law, thereby allowing for a straightforward incorporation of cohesive forces (Mikami, Kamiya & Horio 1998). Despite its wide usage for cohesive flows (e.g. Chaudhuri *et al.* 2006; Anand *et al.* 2009; Figueroa, Li & Mccarthy 2009; Hou, Zhou & Yu 2012; Galvin & Benyahia 2014; Liu *et al.* 2016*b*), the DEM has a large computational overhead compared with other modelling approaches such as continuum theory, preventing its direct application to commercial units and even most laboratory-scale flows (Fullmer & Hrenya 2017; Cocco *et al.* 2017).

The continuum framework provides a more computationally efficient approach for the prediction of cohesive-particle flows, since the solids are treated as a continuous phase via a (single) continuity equation and momentum balance. For non-cohesive rapid flows, constitutive relations for the solids-phase stress are derived based on an analogy with dense-gas kinetic theory (Gidaspow 1994; Jackson 2000; Goldhirsch 2003; Brilliantov & Pöschel 2010; Pannala *et al.* 2011). These closures depend on the granular temperature T_s, which is a measure of the kinetic energy associated with the deviation of particle velocities from the local mean velocity, i.e. $T_s = m_i\langle|\boldsymbol{v}_i - \boldsymbol{u}|^2\rangle/3$, where m_i is the mass and $\boldsymbol{v_i}$ is the instantaneous particle velocity of species i, and $\boldsymbol{u}$ is the local mass-averaged mixture velocity. (The impact of correlated particle velocities due, for example, to clustering instabilities is outside the current scope and is not considered here; interested readers are referred to the reviews of Fox (2014) and Fullmer & Hrenya (2017).) Accordingly, a granular energy balance is also required. Two main approaches have been explored to incorporate the effects of cohesion into this continuum framework. The first approach is via the solution of an algebraic force balance on an agglomerate in order to determine a single agglomerate size within a control volume (i.e. numerical grid cell) (van Wachem & Sasic 2008; Le *et al.* 2009; Wang, van der Hoef & Kuipers 2011; Motlagh *et al.* 2014; Vashisth *et al.* 2015). The equation of continuity, and momentum and granular energy balances are then solved using the single agglomerate size associated with a given control volume. The second approach utilizes a population balance, in which a differential balance on the number density of agglomerates, with source and sink terms representing aggregation and breakage, is solved for each agglomerate size (Ramkrishna 2000). This population balance is then solved in conjunction with the kinetic-theory-based momentum and energy balances. The population-balance approach is more rigorous than its force balance counterpart as it allows for a distribution of agglomerate sizes within a given control volume, yet it requires closures for the source and sink terms

https://doi.org/10.1017/jfm.2017.642 Published online by Cambridge University Press

for agglomerates of different sizes. Many forms of these closures have appeared in the literature, with varying degrees of physical basis. A primary focus of this work is the determination of fundamental closures for the source and sink terms in the population-balance model.

In the population balance, the source and sink terms due to aggregation and breakage are proportional to the product of the number of particles or agglomerates undergoing aggregation or breakage (the number density of pairs) and the aggregation ($\beta(V,\ V')$) or breakage ($\alpha(V,\ V')$) kernels, which represent the frequency of aggregation and breakage events normalized by the number density of pairs (i.e. $n(V)n(V')$). The aggregation and breakage kernels are expected to depend on the frequency of collisions, which can be cast in terms of the (continuum quantity) granular temperature T_s. However, widely used closures for the aggregation kernel include constant kernels or kernels that include the effect of agglomerate size on the collision frequency but not the explicit effect of T_s (for a review, see Cameron *et al.* (2005)). The latter widely used closures utilize a coalescence kernel constant β_0, which the aggregation kernel is directly proportional to. The aggregation kernel is typically given by the product of the constant β_0 and a function of (only) the volumes of the particles or agglomerates undergoing aggregation (Cameron *et al.* 2005). This coalescence kernel constant is generally chosen empirically, and implicitly takes into account the effect of T_s (assumed constant) on the collision frequency. Another, more physically based, aggregation kernel $\beta(V, V')$ is given by the product of the collision frequency and the fraction of collisions that result in aggregation, i.e. the 'success factor' of aggregation ψ_a (Goldschmidt 2001; Tan *et al.* 2004). Fan, Marchisio & Fox (2004) extended this form of $\beta(V, V')$ to breakage, i.e. the product of the collision frequency and the fraction of collisions resulting in breakage ψ_b. Works to date that incorporate the success factors ψ_a and ψ_b have defined ψ_a and ψ_b as a constant (Fan *et al.* 2004; Costa, Folch & Macedonio 2010; Sen & Ramachandran 2013), an empirical fit of system parameters such as mixer shear rate in a granulator (Gantt & Gatzke 2006; Fadda *et al.* 2009) or binary (0 or 1) depending on system conditions such as binder volume fraction in a granulator, as well as cohesion properties (Calvert *et al.* 2009; Le *et al.* 2009; Braumann, Kraft & Mort 2010). An inherent assumption of these approaches is that the outcome of a collision depends on the impact velocity (i.e. the relative velocity between particles at the time of contact), consistent with previous works indicating that relatively low impact velocities lead to aggregation and high impact velocities lead to rebound or breakage (e.g. Seville, Willett & Knight 2000; Gantt & Gatzke 2006; Donahue *et al.* 2012). However, since the distribution of individual particle impact velocities is related to the (continuum) granular temperature T_s, the success factors ψ_a and ψ_b should also depend on T_s. Only one of these works includes the dependence of ψ_a on T_s by setting $\psi_a = 0$ when T_s is above a critical value and $\psi_a = 1$ when T_s is below a critical value (Braumann *et al.* 2010). This approach does not allow the success factor to take intermediate values between 0 and 1. However, a distribution of impact velocities present at a given location, some of which may lead to agglomeration and others of which may not, is the most general case; such a case is represented by an intermediate value of the success factor ($0 < \psi_a < 1$).

It is worthwhile to note that the dependence of the success factor of aggregation ψ_a on the impact velocity or granular temperature T_s has been explored in a few previous works. The fundamental relationship between ψ_a and the impact velocity was first demonstrated by Kantak, Hrenya & Davis (2009), where ψ_a was determined by integrating the normal impact velocity distribution over velocities

https://doi.org/10.1017/jfm.2017.642 Published online by Cambridge University Press

that result in aggregation. While Kantak *et al.* (2009) showed good predictions of ψ_a, their determination depended on the availability of individual (not continuum) collision quantities, namely the distribution of impact velocities, which they obtained from DEM simulations of simple shear flow. In other words, their approach is incompatible with a strictly continuum theory, since individual collision quantities (impact velocities) are unavailable. A method to overcome this shortcoming was recently proposed by Liu (2011), who provided an analytical prediction of the total impact velocity distribution (including normal and tangential components of velocity) as a function of the (continuum quantity) T_s, and determined ψ_a by integrating the distribution over the total impact velocities where agglomeration occurs. This approach, which was based on an assumption that the total impact velocity governs aggregation, was not validated with simulation or experimental data.

An accurate prediction of the success factors ψ_a and ψ_b relies on an accurate estimation of the distribution of impact velocities, and consequently their continuum counterpart, T_s. A crucial term in the granular energy balance is the sink due to inelastic (dissipative) collisions. The amount of dissipation is quantified by the coefficient of restitution e, which is the ratio of the magnitude of the post-collisional normal (head-on) impact velocity of a particle pair to its pre-collisional counterpart. For collisions between cohesive particles, the particles will accelerate towards each other due to the attractive force, undergo a collision at a higher impact velocity than non-cohesive particles, and therefore dissipate more energy (Seville *et al.* 2000). This additional dissipation due to cohesion needs to be taken into account in the granular energy balance. Arastoopour & Kim (2002) accounted for the extra dissipation that occurs during aggregation in their derivation of a kinetic-theory-based continuum theory that accounts for cohesive aggregation only (no breakage). Even for collisions that do not result in aggregation, however, additional energy is also dissipated during collisions between cohesive particles, as demonstrated by numerous previous experiments, theory and simulations (e.g. Davis, Serayssol & Hinch 1986; Thornton & Ning 1998; Weber, Hoffman & Hrenya 2004; Donahue *et al.* 2012; Gollwitzer *et al.* 2012; Murphy & Subramaniam 2017). Another approach for incorporating cohesion into the kinetic theory that accounts for the additional dissipation – whether or not aggregation or breakage occurs – is via the use of an 'effective' coefficient of restitution e_{eff}, which is smaller than the intrinsic coefficient of restitution e_{int} for the material under consideration. Murphy & Subramaniam (2015) used a fundamentally based e_{eff} to solve the granular energy balance in the homogeneous cooling system (HCS). Their continuum theory, however, is restricted to dilute flows undergoing homogeneous cooling.

The first overarching goal of this work, as described in § 2, is to develop a general continuum framework for the rapid flow of solid particles that experience short-range cohesive forces. The specific objectives are twofold: (i) to develop fundamentally based aggregation and breakage kernels including success factors of aggregation ψ_a and breakage ψ_b based on the granular temperature T_s and (ii) to accurately predict T_s for cohesive particles using the granular energy balance. To achieve the first aim, the distribution of normal impact velocities is fundamentally determined as a function of T_s, as we show that the normal component of the impact velocity (rather than the total, as previously assumed (Liu 2011)) solely determines whether agglomeration or rebound occurs during a collision. Then, ψ_a and ψ_b are determined by integrating over the impact velocities at which aggregation and breakage occur. In order to achieve the second aim of accurately predicting T_s, a mean effective coefficient of restitution $\langle e_{eff} \rangle$ is determined based on the distribution of impact velocities and then

https://doi.org/10.1017/jfm.2017.642 Published online by Cambridge University Press

recast in terms of the continuum quantity T_s. The resulting $\langle e_{eff} \rangle$ is then substituted into all of the kinetic-theory-based transport coefficients. Discrete element method simulations of simple shear flow (SSF) are then utilized for verification of the impact velocity distribution developed for the new continuum theory presented here. For the purposes of simplicity, we focus on cohesive granular materials (no gas phase), although the continuum theory can be extended to gas–solid flows in a straightforward manner. In § 2, we develop continuum equations that are general, i.e. they are cast in a manner that does not depend on the specific type of short-range cohesion under consideration. As expected, however, some of the closures contain quantities that are cohesion-specific (e.g. critical velocity of agglomeration) and thus need to be evaluated for the equations to be applied to a specific type of cohesion.

Generally speaking, these cohesion-specific quantities appearing in the population balance (critical velocities $v_{a,V,V',crit}$ and $v_{b,V,V',crit}$, collision diameter $d_{V,V'}$ and daughter distribution $b(V \mid T_s, V', V'')$) and kinetic theory (effective coefficient of restitution e_{eff}) can be found via experiments or particle–particle cohesion models (e.g. Hamaker model for van der Waals forces (Hamaker 1937)). In several previous works involving liquid bridges, each of these cohesion-specific quantities was determined from pendulum experiments (e.g. Davis, Rager & Good 2002; Donahue *et al.* 2010, 2012). For fine particles in which van der Waals forces play an important role ($\lesssim$100 μm diameter for flows in ambient air), however, experimental apparatuses like pendulums (e.g. Donahue *et al.* 2010, 2012) are infeasible due to the small size of the particles. For some forms of cohesion, such challenges can be overcome if the system can be scaled up through non-dimensionalization (i.e. colliding larger particles, which are easier to control and observe, as was done for pendulum experiments involving larger particles) (Donahue *et al.* 2010, 2012). However, a more challenging obstacle is the extension of such experiments to collisions between large agglomerates, in which the control of agglomerate shape and orientation just prior to collision is non-trivial at best. Alternatively, the cohesion-specific quantities ($v_{a,V,V',crit}$, $v_{b,V,V',crit}$, $d_{V,V'}$, $b(V \mid T_s, V', V'')$ and e_{eff}) can be found using force models for particle–particle cohesion (and contact). Although the determination of an accurate cohesion model is challenging due to the extreme sensitivity of the cohesive force to the separation distance and hence particle roughness (Rabinovich *et al.* 2000; Liu *et al.* 2016*a*), such models can be applied in a straightforward manner to collisions involving complex multi-particle agglomerates. More specifically, analytical solutions of cohesion models (Seville *et al.* 2000) for cohesion-specific quantities like e_{eff} have been found for van der Waals forces and capillary forces (e.g. Bryan & Rober Pfeffer 1991; Weber *et al.* 2004), although such analytical solutions are generally tractable only for collisions between single particles. Another approach is to numerically determine the cohesion-specific quantities from controlled two-particle or multi-particle DEM simulations that incorporate the cohesion model, as has been done in many works (e.g. Kafui & Thornton 2000; Ringl *et al.* 2012). Unlike experiments, the simulation of complex collision orientations with larger agglomerates of various shapes is straightforward. Nonetheless, a challenge of such controlled simulations is that the most frequent types of collision orientations are not known *a priori* for a given flow system. Another option, which has not been explored yet, is the determination of the cohesion-specific quantities, $v_{a,V,V',crit}$, $v_{b,V,V',crit}$, $d_{V,V'}$, $b(V \mid T_s, V', V'')$ and e_{eff}, from relatively simple DEM simulations of many-particle flows (e.g. simple shear flow). This approach has the advantage of sampling the collision orientations from a simplified flow expected to have similar orientation characteristics to the ultimate flow of interest (e.g. shear-driven system). This approach, alongside simulations of controlled two-particle collisions, will be explored in this work.

https://doi.org/10.1017/jfm.2017.642 Published online by Cambridge University Press

Accordingly, the second overarching goal of this work is to determine the cohesion-specific quantities needed for the new theory to be fully specified and to be applied to practical situations, as described in §§ 3 and 4. Specific objectives of this second portion of the work are to (iii) demonstrate the determination of the cohesion-specific quantities ($v_{a,V,V',crit}$, $v_{b,V,V',crit}$, $d_{V,V'}$, $b(V \mid T_s, V', V'')$ and e_{eff}) needed for the closure of the new continuum theory derived in § 2 via consideration of a specific source of cohesion and (iv) provide initial validation for the resulting fully specified continuum theory. For simplicity, the focus here will be on granular systems (no fluid phase); extension of kinetic-theory balances to multiphase flows is well documented elsewhere (e.g. Gidaspow 1994; Jackson 2000; Pannala *et al.* 2011). Moreover, we consider van der Waals cohesion, although the methods demonstrated here to obtain the cohesion-specific quantities can be applied to other mechanisms of cohesion. Finally, we restrict ourselves to lightly cohesive systems with only single particles and two-particle agglomerates (singlets and doublets respectively). This simplification essentially isolates any sources of error in the predictions to those stemming from the new closures derived here. With regards to the approach for objective (iii), controlled two-particle DEM simulations are used to determine the critical velocity of aggregation $v_{a,V,V',crit}$ and the effective coefficient of restitution e_{eff}, and SSF simulations are used to determine the critical velocity of breakage $v_{b,V,V',crit}$ and the collision cylinder diameter $d_{V,V'}$. The population-balance closures are then verified (coding accuracy) using SSF and validated (theory accuracy) using the HCS. Further, the appropriateness of using $\langle e_{eff} \rangle$ in kinetic-theory expressions is demonstrated in both the SSF and the HCS.

2. Theory development

2.1. *Population balance*

In the population balance, each agglomerate size is treated as its own species, with a separate balance equation on the number density of that species. In its most general form, the population balance is given by (Ramkrishna 2000)

$$\frac{\partial}{\partial t}[n(V,t)] + \boldsymbol{\nabla} \cdot [\boldsymbol{u}(V,t)n(V,t)] = S(V,t) \tag{2.1}$$

for an agglomerate of volume V with a number density of n and velocity $\boldsymbol{u}$. The left-hand side represents the transient and convective contributions, while the right-hand side represents the source and/or sinks of agglomerates of volume V. More specifically, the net generation, S, is defined as (Ramkrishna 2000)

$$S(V,t) = B_a(V,t) - D_a(V,t) + B_b(V,t) - D_b(V,t), \tag{2.2}$$

where B_a is the volumetric birth rate due to aggregation, D_a is the death rate due to aggregation, B_b is the birth rate due to breakage and D_b is the death rate due to breakage. It should be noted that birth and death due to nucleation (coalescence due to a phase change or chemical reaction) are not considered here, as the focus of this work is on the aggregation and breakage kernels.

The birth rate due to aggregation used here is similar to that generally given in the literature (Ramkrishna 2000), and is defined as

$$B_a(V,t) = \frac{1}{2}\int_0^V (1+\delta_{V-V',V'})\beta(V', V-V', t)n(V-V',t)n(V',t)\,\mathrm{d}V, \tag{2.3}$$

https://doi.org/10.1017/jfm.2017.642 Published online by Cambridge University Press

where $\beta(V', V - V', t)$ is the 'aggregation kernel', which represents the frequency of aggregation events (i.e. when two agglomerates collide and form a larger agglomerate) between agglomerates of sizes V' and $V - V'$, per unit volume and per number density of each agglomerate size undergoing aggregation. Here, $\delta_{V-V',V'}$ is the Kronecker delta function,

$$\delta_{V-V',V'} = \begin{cases} 0, & V - V' \neq V', \\ 1, & V - V' = V'. \end{cases} \tag{2.4}$$

It is worthwhile to note that $1 + \delta_{V-V',V}$ ensures the proper counting of birth due to aggregation events during symmetric aggregation (i.e. the case of $V' = V - V'$ is only summed over by the integrand in (2.3) once, whereas all other combinations $V' \neq V - V'$ are summed over twice), and does not appear in prior works. It should also be noted that the birth rate due to aggregation given in (2.3) only accounts for aggregation events in which all of the particles in the agglomerates of sizes V' and $V - V'$ form an agglomerate of size V; collisions involving simultaneous aggregation and breakage in which an agglomerate of size V is formed are accounted for in the birth rate due to breakage (B_b), as detailed below.

Similarly, the rate of death rate due to aggregation is taken as

$$D_a(V, t) = \int_0^\infty (1 + \delta_{V,V'})\beta(V, V', t)n(V, t), n(V', t)\,\mathrm{d}V', \tag{2.5}$$

where $\delta_{V,V'}$ is the corresponding Kronecker delta function. Again, the $1 + \delta_{V,V'}$ term is not included in prior works. This term is included here to represent the events in which two agglomerates of size V collide and aggregate, thereby leading to the death of two agglomerates of size V.

Before presenting the equations for the birth and death rates due to breakage (B_b and D_b), it is worth noting that an agglomerate can break due to (i) collision with another agglomerate, (ii) collision with a wall, (iii) shear forces from a surrounding fluid or (iv) centrifugal forces arising from its own rotation (Ramachandran *et al.* 2009; Donahue *et al.* 2012). Mechanism (i) is the focus of this work, although the approach taken here could easily be extended to mechanism (ii). Consequently, the birth and death rates due to breakage will take a form that is proportional to the frequency of collisions between two agglomerates, and hence the concentration of each (similar to the birth and death rates due to aggregation, B_a and D_a).

The birth rate due to breakage is defined similarly to previous works (Fan *et al.* 2004) as

$$B_b(V, t) = \int_0^\infty \int_0^\infty \left(\frac{1 + \delta_{V',V''}}{2}\right) \alpha(V', V'')b(V \mid T_s, V', V'')n(V', t)n(V'', t)\,\mathrm{d}V'\,\mathrm{d}V'', \tag{2.6}$$

where $\alpha(V', V)$ is the breakage kernel representing the frequency of breakage events between agglomerates of sizes V' and V''. The quantity $b(V \mid T_s, V', V'')$ is the daughter distribution function, which gives the number of agglomerates of size V produced by a collision resulting in any breakage of agglomerates of size V' and V'' for a system of mixture granular temperature T_s (i.e. a measure of the fluctuating kinetic energy of particles and agglomerates). The term $(1 + \delta_{V',V''})/2$ is included to prevent double counting of breakage events due to the second integral.

Finally, the death rate due to breakage (Fan *et al.* 2004) is given by

$$D_b(V, t) = \int_0^\infty \alpha(V, V')n(V, t)n(V', t)\,\mathrm{d}V'. \tag{2.7}$$

https://doi.org/10.1017/jfm.2017.642 Published online by Cambridge University Press

In this work, the aggregation kernel β used in (2.3) and (2.5) and the breakage kernel α used in (2.6) and (2.7) are defined in a similar manner to previous literature (Goldschmidt 2001). A notable exception is that the breakage kernel α is now also dependent on the frequency of collisions (Fan *et al.* 2004),

$$\beta(V, V') = \psi_a(V, V')\frac{\omega(V, V')}{n(V)n(V')}, \tag{2.8}$$

$$\alpha(V, V') = \psi_b(V, V')\frac{\omega(V, V')}{n(V)n(V')}, \tag{2.9}$$

where $\psi_a(V, V')$ and $\psi_b(V, V')$ are the 'success factors' of aggregation and breakage respectively, which represent the fraction of collisions that result in agglomeration or breakage. Here, $\omega(V, V')$ is the collision frequency per unit volume of agglomerates of size V and V', given by

$$n(V)n(V')\pi d_{V,V'}^3 g_0 \left[\frac{4}{d_{V,V'}}\left(\frac{T_s}{\pi}\frac{m_V\,\mathrm{dof}_{V'} + m_{V'}\,\mathrm{dof}_V}{m_V m_{V'}}\right)^{1/2} - \frac{2}{3}(\boldsymbol{\nabla}\cdot\boldsymbol{u}_s)\right], \tag{2.10}$$

T_s is the granular temperature (which represents the variance of the velocities of individual particles relative to the local motion), m_V is the mass of an agglomerate of size V, g_0 is the radial distribution function (e.g. that given by Carnahan Starling (Mansoori 1971)) and $d_{V,V'}$ is the collision cylinder diameter of agglomerates of sizes V and V'. A collision cylinder diameter interpretation is adopted here as agglomerates are aspherical, and thus whether or not they are in contact (undergoing a collision) is no longer a function of just position, but also orientation. The term dof_V represents the sum of translational and rotational degrees of freedom of an agglomerate of size V (e.g. for frictionless particles, a singlet has three translational degrees of freedom and $\mathrm{dof}_1 = 3$, a doublet has three translational and two rotational degrees of freedom and $\mathrm{dof}_2 = 5$). It should be noted that this expression for the collision frequency does not take into account interphase slip, and does not assume the system to be homogeneous. In the validation systems explored here, there is no interphase slip and the system is homogeneous, so this expression is applicable.

To recap, the population-balance equations for each agglomerate size (2.1) include sink and source terms for the rates of birth and death due to aggregation and breakage (2.3), (2.5)–(2.7). The fundamental closures for the sink and source terms depend on the aggregation and breakage kernels, β and α respectively, i.e. the frequency of aggregation and breakage events (2.8)–(2.9). The kernels now require a closure for the success factors of aggregation and breakage (ψ_a and ψ_b).

2.2. *Population-balance closures: success factors of aggregation* (ψ_a) *and breakage* (ψ_b)

As mentioned above, the closures for the aggregation ($\beta(V, V')$) and breakage ($\alpha(V, V')$) kernels are proportional to the fraction of collisions that result in aggregation or breakage, or the success factors ψ_a and ψ_b. Numerous previous works (e.g. Lian, Thornton & Adams 1998; Jackson 2000; Calvert *et al.* 2009; Donahue *et al.* 2010, 2012; Ringl *et al.* 2012) have demonstrated that the result of a collision between two cohesive bodies (single particles and/or agglomerates) depends on their impact (relative) velocity. Moreover, a series of numerical simulations of two-particle collisions of cohesive particles indicates that there is a normal component of the

https://doi.org/10.1017/jfm.2017.642 Published online by Cambridge University Press

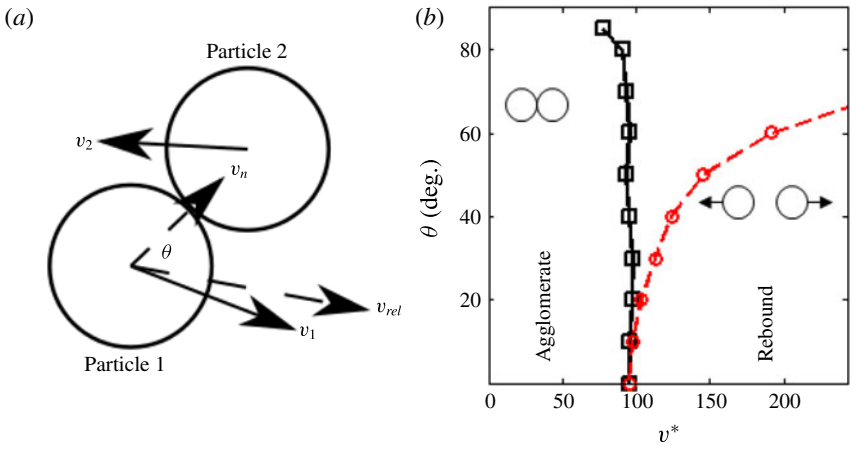


FIGURE 1. (Colour online) (*a*) Collision schematic; $\boldsymbol{v}_{rel} = \boldsymbol{v}_1 - v_2$. (*b*) Regime map of binary collisions between two cohesive primary particles (singlets). Here, v^* is a non-dimensionalized impact velocity ($=v/(A/(\rho d_1^3))^{1/2}$, where A is the Hamaker constant). The black line and points show the magnitude of the normal component of the critical impact velocity ($v^*_{a,1,1,crit}$), which demarcates aggregation and rebound from DEM simulations of cohesive particles described in § 3.2.1. The red dashed line and points show the magnitude of the critical total relative impact velocity ($v^*_{a,tot,1,1,crit}$). It should be noted that the normal component $v^*_{a,1,1,crit}$ is approximately independent of the impact angle, whereas the total component $v^*_{a,tot,1,1,crit}$ is not.

impact velocity, v_n, which demarcates the agglomeration and breakage outcomes, as illustrated in figure 1 (black solid line), which is consistent with past experimental observations for cohesion due to liquid (Donahue *et al.* 2010, 2012). Accordingly, ψ_a and ψ_b should depend on the distribution of v_n in a given system. In terms of continuum variables, the distribution of individual collision impact velocities is related to the (continuum) granular temperature, since the latter is a measure of the particle velocity distribution relative to the local mean velocity (i.e. a measure of particle velocity fluctuations). Therefore, the closures for the success factors ψ_a and ψ_b should depend on T_s.

Expressions similar to previous works (Kantak *et al.* 2009; Liu 2011) are used to calculate the success factors of both agglomeration and breakage. Namely, the success factors are defined here as

$$\psi_a(V, V') = \int_0^{v_{a,V,V',crit}} f(v_n)\,\mathrm{d}v_n, \tag{2.11}$$

$$\psi_b(V, V') = \int_{v_{b,V,V',crit}}^{\infty} f(v_n)\,\mathrm{d}v_n, \tag{2.12}$$

where $v_{a,V,V',crit}$ and $v_{b,V,V',crit}$ are the critical normal impact velocities of agglomeration and breakage for collisions between agglomerates of sizes V and V' respectively. For the purposes of generality, the critical velocities of agglomeration and breakage are allowed to take on different values for a given pair of colliding objects (i.e. the critical velocities of agglomeration and breakage are different from each other), as well as for different sizes of agglomerates undergoing collisions. Here, $f(v_n)$ is the normalized probability density function that a collision between

https://doi.org/10.1017/jfm.2017.642 Published online by Cambridge University Press

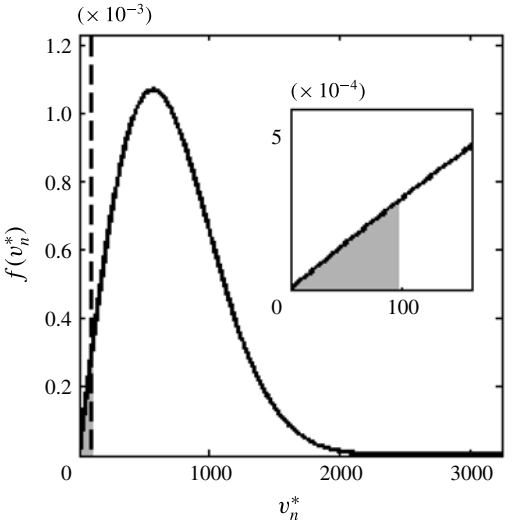


FIGURE 2. Illustrative schematic of prediction of the success factor of aggregation for particles. The solid black line shows the normal impact velocity distribution $f(v_n)$. The dashed black line shows the critical velocity of aggregation $v_{a,V,V',crit}$. The grey area, which is shown expanded in the inset, is the success factor of aggregation ψ_a.

agglomerates will have a normal impact velocity of v_n. This method for calculating the success factors is depicted graphically in figure 2 for ψ_a. For a given system, the critical velocities of agglomeration (vertical dashed line in figure 2) and breakage depend on the type of cohesion (van der Waals, liquid bridging, etc.) and materials involved, and can be determined mathematically from a particle–particle cohesion model (i.e. analytical solutions to two-body collisions or the DEM (e.g. Bryan & Rober Pfeffer 1991; Weber *et al.* 2004)) or from experiments (e.g. Donahue *et al.* 2012). Accordingly, general expressions for the success factors as functions of these critical velocities can be determined if $f(v_n)$ is known. Kantak *et al.* (2009) determined $f(v_n)$ from a Gaussian fit of DEM data, which confirmed the accuracy of the expressions above but is not useful in a general continuum framework since the impact velocities are quantities specific to an individual collision (i.e. not continuum quantities) and thus remain unknown. Instead, we derive an analytical prediction of $f(v_n)$ as a function of the granular temperature, a flow variable that is solved for within the continuum framework. Liu (2011) analytically determined the distribution of total relative velocity (v_{tot}) as a function of the granular temperature T_s. However, figure 1 demonstrates that it is more appropriate to consider only the normal component of the impact velocity, for which the critical value is constant across various impact angles (θ). Put another way, considering ψ as a function of v_n only, instead of ψ as a function of v_{tot} and θ, is much cleaner since the θ distribution (also comprising quantities specific to individual collisions and not solved for in the continuum framework) does not have to be assumed or estimated. In the following, a novel analytical closure for $f(v_n)$ is derived as a function of T_s.

Assuming a Maxwellian distribution of particle velocities and independence of each velocity component for agglomerates of size V, the magnitude of the velocity

https://doi.org/10.1017/jfm.2017.642 Published online by Cambridge University Press

distribution of the agglomerate (or single particle) is given by

$$p(\boldsymbol{v}) = p(v_x)p(v_y)p(v_z) = \frac{1}{\sqrt{2\pi\sigma_{\boldsymbol{u}}^2}} \exp\left[-\frac{(\boldsymbol{v}-\boldsymbol{u})^2}{2\sigma_{\boldsymbol{u}}^2}\right], \tag{2.13}$$

where $\boldsymbol{v}$ is the agglomerate translational velocity, $\boldsymbol{u}$ is the local mean velocity of the agglomerates of the same size and v_x, v_y, v_z are the x, y and z components of the agglomerate translational velocity respectively. The term $\sigma_{\boldsymbol{u}}^2$ is the variance of the magnitude of velocities of agglomerates of the same size. It is related to the granular energy E and granular temperature by

$$E = 3T_{s,V}/2 = \mathrm{dof}_V m_V \sigma_{\boldsymbol{u}}^2/6. \tag{2.14}$$

The assumption of isotropy gives

$$p(v_x) = p(v_y) = p(v_z). \tag{2.15}$$

It should be noted that the incorporation of anisotropy is highly non-trivial (Sela & Goldhirsch 1998), and it may not be necessary to incorporate it in the theory even when such higher-order effects are present (Mitrano *et al.* 2013; Fullmer & Hrenya 2017). Further, the SSF and HCS explored in the current work are isotropic. Application of (2.15) to (2.13) yields

$$p(\boldsymbol{v}) = p(v_x)^3 = \frac{1}{\sqrt{2\pi\sigma_{\boldsymbol{u}}^2}} \exp\left[-\frac{3(v_x-u_x)^2}{2\sigma_{\boldsymbol{u}}^2}\right], \tag{2.16}$$

where u_x is the mean velocity of the agglomerate size in the x direction. By solving (2.14) for $\sigma_{\boldsymbol{u}}^2$, and substituting $\sigma_{\boldsymbol{u}}^2$ and (2.16) into (2.13), the velocity distribution for a single agglomerate (or particle) in one direction becomes

$$p(v_x) = \frac{1}{\sqrt{6\pi T_{s,V}/(m_V\,\mathrm{dof}_V)}} \exp\left[-\frac{(v_x-u_x)^2}{6T_{s,V}/(m_V\,\mathrm{dof}_V)}\right], \tag{2.17}$$

where p is the normalized probability distribution function, v_x is the x component of the velocity of an individual agglomerate and u_x is the x component of the local mean species velocity. Assuming that particles and/or agglomerates of different masses display an approximate equipartition of energy ($T_{s,V} = T_{s,V'} \equiv T_s$), (2.17) can be rewritten for two agglomerates of different masses V and V' as

$$p(v_{x,V}) = \frac{1}{\sqrt{6\pi T_s/(m_V\,\mathrm{dof}_V)}} \exp\left[\frac{-(v_{x,V}-u_{x,V})^2}{6T_s/(m_V\,\mathrm{dof}_V)}\right], \tag{2.18}$$

$$p(v_{x,V'}) = \frac{1}{\sqrt{6\pi T_s/(m_{V'}\,\mathrm{dof}_{V'})}} \exp\left[\frac{-(v_{x,V'}-u_{x,V'})^2}{6T_s/(m_{V'}\,\mathrm{dof}_{V'})}\right]. \tag{2.19}$$

By manipulating (2.19) (redefining the coordinate system to replace $v_{x,V'}$ with $-v_{x,V'}$ and $u_{x,V'}$ with $-u_{x,V'}$ throughout), the following is obtained:

$$p(-v_{x,V'}) = \frac{1}{\sqrt{6\pi T_s/(m_{V'}\,\mathrm{dof}_{V'})}} \exp\left[\frac{-(-v_{x,V'}+u_{x,V'})^2}{6T_s/(m_{V'}\,\mathrm{dof}_{V'})}\right]. \tag{2.20}$$

https://doi.org/10.1017/jfm.2017.642 Published online by Cambridge University Press

Combining the two Gaussians (2.18) and (2.20), and assuming molecular chaos (velocities of colliding particles are not correlated) gives

$$p(v_{x,V}-v_{x,V'})=\sqrt{\frac{1}{2\pi T_s\left[\frac{3}{m_V\,\mathrm{dof}_V}+\frac{3}{m_{V'}\,\mathrm{dof}_{V'}}\right]}}\exp\left[\frac{-(v_{x,V}-v_{x,V'}+u_{x,V}-u_{x,V'})^2}{2T_s\left[\frac{3}{m_V\,\mathrm{dof}_V}+\frac{3}{m_{V'}\,\mathrm{dof}_{V'}}\right]}\right]. \tag{2.21}$$

It should be noted that this expression includes interphase slip, and assumes that the system is homogeneous. These assumptions are appropriate in the validation systems explored here as there is no interphase slip and these systems are homogeneous. It should also be noted that the direction x is arbitrary, so it is defined as the normal direction between the centres of mass of agglomerates of sizes V and V',

$$v_{x,V}-v_{x,V'}=v_n. \tag{2.22}$$

In (2.21), the difference in mean velocities in the x (normal) direction is the magnitude of the relative velocity between the agglomerate sizes,

$$u_{x,V}-u_{x,V'}=|\boldsymbol{u}_V-\boldsymbol{u}_{V'}|, \tag{2.23}$$

where $\boldsymbol{u}_V$ and $\boldsymbol{u}_{V'}$ are the mean velocities of agglomerates of sizes V and V'. The distribution of normal velocities between agglomerates of sizes V and V' is therefore given by

$$p(v_n)=\sqrt{\frac{1}{2\pi T_s\left[\frac{3}{m_V\,\mathrm{dof}_V}+\frac{3}{m_{V'}\,\mathrm{dof}_{V'}}\right]}}\exp\left[\frac{-(v_n+|\boldsymbol{u}_V-\boldsymbol{u}_{V'}|)^2}{2T_s\left[\frac{3}{m_V\,\mathrm{dof}_V}+\frac{3}{m_{V'}\,\mathrm{dof}_{V'}}\right]}\right]. \tag{2.24}$$

In order to get the impact velocity distribution $f(v_n)$, three additional terms (C, $H(v_n)$ and $\omega(v_n)$) must be multiplied by the distribution of normal velocities,

$$f(v_n)=CH(v_n)\omega(v_n)p(v_n), \tag{2.25}$$

where

$$H(v_n)=\begin{cases}0, & v_n<0,\\ 1, & v_n\geqslant 0.\end{cases} \tag{2.26}$$

Inclusion of the Heaviside function, $H(v_n)$, removes the relative velocities of particles moving away from one another (i.e. negative impact velocities) from the distribution as there is no chance of a collision occurring. Here, C is a normalization constant which ensures that the distribution is normalized,

$$\int_{-\infty}^{\infty}f(v_n)\,\mathrm{d}v_n=1. \tag{2.27}$$

Therefore, C is found by substituting (2.25) into (2.27) and rearranging,

$$C=\frac{1}{\int_{-\infty}^{\infty}H(v_n)\Omega(v_n)p(v_n)\,\mathrm{d}v_n}. \tag{2.28}$$

https://doi.org/10.1017/jfm.2017.642 Published online by Cambridge University Press

The term $\Omega(v_n)$ accounts for the fact that impacts between particles with higher normal velocities will occur more frequently,

$$\Omega(v_n) = \frac{1}{P(v_n)}, \tag{2.29}$$

where $P(v_n)$ is the time it takes for two particles destined to collide to approach one another, given by

$$P(v_n) = \frac{l_{arb}}{v_n}. \tag{2.30}$$

Here, l_{arb} is the arbitrary distance between the particles when they begin to approach one another. By substituting (2.26), (2.28), (2.29) and (2.30) into (2.25), the distribution of impact velocities becomes

$$f(v_n) = \frac{C_{norm} v_n}{2\pi T_s \varsigma} \exp\left[\frac{-(v_n + |\boldsymbol{u}_V - \boldsymbol{u}_{V'}|)^2}{2T_s\varsigma}\right] H(v_n), \tag{2.31}$$

where

$$\varsigma = \frac{3}{m_V \,\mathrm{dof}_V} + \frac{3}{m_{V'}\,\mathrm{dof}_{V'}} \tag{2.32}$$

and (2.28) is used to obtain the normalization constant,

$$C_{norm} = \frac{C}{l_{arb}} = \frac{T_s\varsigma}{|\boldsymbol{u}_V - \boldsymbol{u}_{V'}|\sqrt{\frac{\pi T_s\varsigma}{2}}\left[1 + \sqrt{\varsigma}\,\mathrm{erf}\left(\frac{|\boldsymbol{u}_V - \boldsymbol{u}_{V'}|}{\sqrt{2T_s\varsigma}}\right)\right] + \varsigma \exp\left(\frac{-|\boldsymbol{u}_V - \boldsymbol{u}_{V'}|^2}{2T_s\varsigma}\right)}. \tag{2.33}$$

Further, it should be noted that in the special case where the mean velocities of the two particle types in question are the same (i.e. $|\boldsymbol{u}_V - \boldsymbol{u}_{V'}| = 0$, and also the case when $V' = V$), then $C_{norm} = 1$ and $f(v_n) = (v_n/T_s\varsigma)\exp[-v_n^2/2T_s\varsigma]H(v_n)$.

The derivation of $f(v_n)$ presented above is validated in figure 3 via DEM simulations of an SSF system (see § 3.2.2 for details on the method), in which the granular temperature is constant and the local mean velocities of each agglomerate size are equal. The impact velocities were measured just prior to collision in the DEM. Moreover, to isolate any error associated with the new derivation, the T_s measured in the DEM was used as an input to the predictions for the impact velocity distribution (instead of solving for T_s using continuum theory) for both the current work (2.34) and the previous prediction for the total impact velocity given by Liu (2011). The results indicate that the prediction of $f(v_n)$ from the current work adequately captures the normal component of the impact velocity distribution observed in the DEM simulations. It is also worth noting that the prediction for the total component of the impact velocity distribution derived by Liu (2011) also matches well with the corresponding DEM data. However, as demonstrated below in figure 9 and alluded to above, the use of the total component of the impact velocity results in an inaccurate prediction of the success factor due to the dependence of its critical velocity on the impact angle, whereas the normal component of the critical velocity is independent of the impact angle (figure 1).

The distribution of impact velocities, $f(v_n)$, in (2.31) can now be integrated with respect to v_n according to (2.11) and (2.12) in order to give the success factors.

https://doi.org/10.1017/jfm.2017.642 Published online by Cambridge University Press

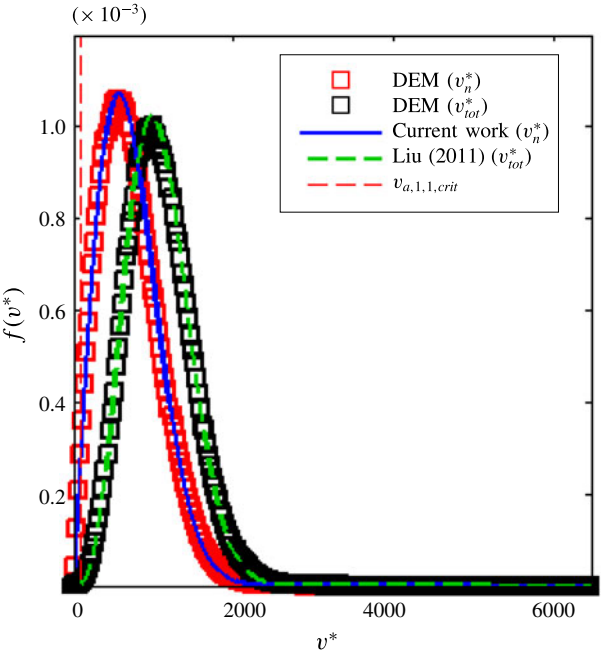


FIGURE 3. (Colour online) Comparison of normal impact velocity distributions $f(v_n)$ predicted by continuum theory (2.13) and the DEM for singlet–singlet collisions (see § 3.2.2 for more details) in SSF (solid volume fraction $\varepsilon_s = 0.1$, shear rate $\gamma^* = \gamma d_1 / v_{a,1,1,crit} = 1.08$). It should be noted that Liu (2011) predicts the total impact velocity (v_{tot}^*) rather than the normal impact velocity (v_n^*).

This integration will eliminate v_n, a variable not present in the continuum theory, and yield a success factor that depends on T_s, $\boldsymbol{u}_V$ and $\boldsymbol{u}_{V'}$, with each of these determined from kinetic-theory-based balances present in the continuum theory.

In addition to the constitutive quantities and their related variables described above (B_a, D_a, B_b, D_b, β, α, ψ_a, ψ_b, b, $f(v_n)$), several parameters are still needed to fully close the population balance and kinetic-theory-based balances; namely, the cohesion-specific parameters include the critical velocities of agglomeration ($v_{a,V,V',crit}$) and breakage ($v_{b,V,V',crit}$) appearing in (2.11)–(2.12), the collision cylinder diameter $d_{V,V'}$ (2.8)–(2.9) and the daughter distributions $b(V \mid T_s, V', V'')$ appearing in (2.6). The closures for the population balance presented in this section are dependent on T_s, $\boldsymbol{u}_V$ and $\boldsymbol{u}_{V'}$, and thus appropriate balances are needed to determine these flow-field variables, as detailed below.

2.3. *Momentum and granular energy balances*

The solids-phase momentum balance for monodisperse inelastic spheres takes the general form (Gidaspow 1994)

$$\frac{\partial (mn\boldsymbol{u})}{\partial t} + \boldsymbol{\nabla} \cdot (mn\boldsymbol{u}\boldsymbol{u}) = -\boldsymbol{\nabla} \cdot (P\boldsymbol{I} + \boldsymbol{\tau}) + \boldsymbol{F}_{body}, \tag{2.34}$$

where P is the granular pressure, $\boldsymbol{\tau}$ is the solids stress tensor and $\boldsymbol{F}_{body}$ is the body force vector.

https://doi.org/10.1017/jfm.2017.642 Published online by Cambridge University Press

Equation (2.34) describes the momentum balance of a monodisperse system. Since a distribution of agglomerate sizes is expected in a given system, a polydisperse kinetic theory (Garzó, Dufty & Hrenya 2007*a*; Garzó, Hrenya & Dufty 2007*b*; Hrenya 2011) is expected to be most appropriate. Polydispersity is not relevant for the demonstration case presented here, however, as we target a lightly cohesive system in order to isolate the new aspects of our theory and thus more easily identify the source of any discrepancies. Accordingly, a monodisperse approximation is appropriate for our current purposes.

Similarly, the granular energy balance takes the following form:

$$\frac{\partial(\frac{3}{2}nT_s)}{\partial t} + \nabla\cdot\left(\frac{3}{2}nT_s\boldsymbol{u}\right) = -(P\boldsymbol{I}+\boldsymbol{\tau}):(\nabla\boldsymbol{u}) - \nabla\cdot\boldsymbol{q} - \zeta T_s, \tag{2.35}$$

where $-(P\boldsymbol{I}+\boldsymbol{\tau}):(\nabla\boldsymbol{u})$ gives the generation of granular energy due to shear, $\boldsymbol{q}$ is the flux of granular energy and ζ is the dissipation rate (all of which are dependent on the granular temperature and coefficient of restitution). It should be recalled that no fluid effects are given in (2.34) or (2.35), as the current focus is on a granular system, with the intent of isolating the new aspects of our theory.

To close the momentum and granular energy balances, closures are required for P, $\boldsymbol{\tau}$, $\boldsymbol{q}$ and ζ. These closures are generally obtained using an analogy with dense-gas kinetic theory – i.e. based on the Chapman–Enskog expansion of the Enskog equation, which is modified to account for the inelasticity of the particles (Hrenya 2011). These closures depend on particle properties such as e_{int}, as well as flow variables such as T_s, ε_s and $\boldsymbol{u}$. Explicit closures can be found in detail elsewhere (e.g. Garzó & Dufty (1999) for a monodisperse system). In a cohesive system, agglomerate shape is expected to have an effect on these closures, which are based on an assumption of spherical particles. Rigorous inclusion of these effects is outside the scope of this work, and is not relevant for the lightly cohesive approximately monodisperse system examined here. Accordingly, the focus of kinetic-theory modifications considered here will remain on the effects of cohesion on the coefficient of restitution.

2.4. *Closure of kinetic-theory-based balances: effective restitution coefficient*

As discussed earlier, collisions between cohesive particles are more dissipative than collisions between non-cohesive particles due to the added acceleration experienced by approaching particles with attractive forces. For non-cohesive particles, the (intrinsic) coefficient of restitution is defined as the absolute value of the ratio of the post-collision normal relative velocity $v_{n,f}$ and the pre-collision normal relative velocity $v_{n,0}$ of two colliding particles ($e_{int} = |v_{n,f}/v_{n,0}|$), and is an input to the kinetic-theory-based closures for the transport coefficients. For elastic particles, $e_{int} = 1$, and for inelastic particles, $0 < e_{int} < 1$. For cohesive particles, the additional dissipation decreases the value of $|v_{n,f}/v_{n,0}|$ to some effective value, e_{eff}, which depends on the velocity at which the particles collide (Davis *et al.* 2002; Donahue *et al.* 2010; Gollwitzer *et al.* 2012; Abbasfard, Evans & Moreno-Atanasio 2016); at infinitely high impact velocities, $e_{eff} \to e_{int}$.

To account for cohesion, we seek to use an impact-velocity-dependent coefficient of restitution, ultimately cast in terms of its continuum counterpart T_s. First, the dependence of e_{eff} on v_n can be determined from experiments or DEM simulations; an illustrative example is shown in the dotted line of figure 4 for the case of van der Waals forces. Aggregation occurs when $e_{eff} = 0$ and rebound occurs when $e_{eff} > 0$.

https://doi.org/10.1017/jfm.2017.642 Published online by Cambridge University Press

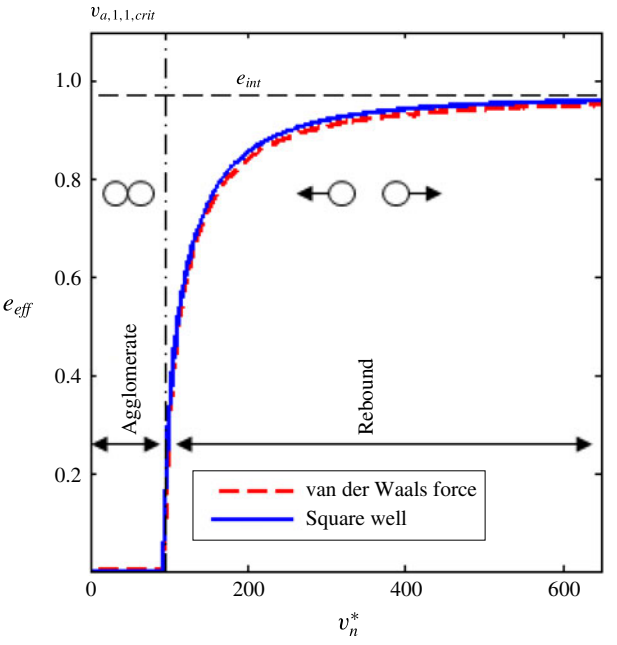


FIGURE 4. (Colour online) Effective coefficient of restitution measured in DEM simulations of collisions between two particles with van der Waals forces described in § 3.2.1 (red dashed line) compared with the prediction from the square-well model ((2.36), blue solid line), as well as the intrinsic property value (black dashed line).

This dependence can be captured via a numerical fit of the data from experiments or the DEM. Alternatively, an analytical approximation based on the square-well model is used here for purposes of simplicity. In particular, an analytical prediction for e_{eff} is available for cohesive hard spheres described by a square well (Weber *et al.* 2004),

$$e_{eff}(v_n) = H(v_n)\sqrt{e_{int}^2 + \frac{(e_{int}^2 - 1)D_{well}}{4mv_n^2}}, \tag{2.36}$$

where e_{int} is the intrinsic (non-cohesive) coefficient of restitution, assumed to be constant for this work, and D_{well} is the well depth, given by Weber *et al.* (2004),

$$D_{well} = \frac{4mv_{a,crit}^2 e_{int}^2}{1 - e_{int}^2}. \tag{2.37}$$

Figure 4 shows a comparison of e_{eff} predicted by the square-well model with that observed in two-particle simulations (DEM) of particles subject to van der Waals cohesion. The results indicate that the analytical prediction of e_{eff} based on the square-well model agrees quantitatively well with the DEM data. Further, the expression for $e_{eff}(v_n)$ given by the square-well model (2.36) is expected to be extendible to other types of cohesion where the e_{eff} versus v_n plot takes on the same general shape – e.g. liquid bridging experiments (Davis *et al.* 2002; Weber *et al.* 2004; Liu *et al.* 2016*c*).

Rigorous incorporation of an impact-velocity-dependent coefficient of restitution, as illustrated in figure 4, into the derivation of the transport coefficients is non-trivial

https://doi.org/10.1017/jfm.2017.642 Published online by Cambridge University Press

at best even for simple systems (Murphy & Subramaniam 2015), and is outside the current scope. Another approach to account for the additional dissipation due to cohesion is by using a mean value of the effective coefficient of restitution e_{eff}, or $\langle e_{eff}\rangle$, in the transport coefficients and dissipation rate. This value of $\langle e_{eff}\rangle$, like e_{eff} itself, lies in the range $0 < \langle e_{eff}\rangle < e_{int}$. Whereas Murphy & Subramaniam (2015) used e_{eff} in the dissipation term in the granular energy balance, here, $\langle e_{eff}\rangle$ is instead calculated and utilized in all of the kinetic-theory-based closures. The mean effective coefficient of restitution is calculated via

$$\langle e_{eff}\rangle = \frac{\displaystyle\int_{v_{a,crit}}^{\infty} e_{eff}(v_n) f(v_n)\,\mathrm{d}v_n}{\displaystyle\int_{v_{a,crit}}^{\infty} f(v_n)\,\mathrm{d}v_n}, \tag{2.38}$$

where $f(v_n)$ is defined above in terms of T_s (see (2.31)) and $e_{eff}(v_n)$ is dictated by the specific type of cohesion under consideration. It should be noted that this integrand has no analytical solution and must be integrated numerically for each numerical cell in the domain of a given system.

3. Methods

3.1. *Discrete element method*

An in-house code was used to perform the DEM simulations. The position $\boldsymbol{x}$ and velocity $\boldsymbol{v}$ of each particle were updated according to Newton's second law of motion, using Euler integration. The forces acting on the particles are given by

$$\boldsymbol{F} = \boldsymbol{F}_{coh} + \boldsymbol{F}_{cont}. \tag{3.1}$$

Here, $\boldsymbol{F}$ is the sum of the cohesive ($\boldsymbol{F}_{coh}$) and contact ($\boldsymbol{F}_{cont}$) forces acting on the particle (no external forces are considered in this work). For simplicity, particle friction was not included in this study, and thus the angular momentum balance was not included.

The Hertzian contact model gives the magnitude of the contact force (Antypov & Elliott 2011),

$$F_{cont} = \begin{cases} \dfrac{4E_{eff}\sqrt{R_{eff}}}{3}\delta^{3/2} + \eta\dfrac{\mathrm{d}\delta}{\mathrm{d}t}, & \delta \geqslant 0, \\ 0, & \delta < 0, \end{cases} \tag{3.2}$$

where δ is the overlap of the two particles and

$$E_{eff} = \frac{E_i E_j}{E_i(1+\nu_j^2) + E_j(1+\nu_i^2)}, \tag{3.3}$$

$$R_{eff} = \frac{R_i R_j}{R_i + R_j}, \tag{3.4}$$

$$\eta = \frac{-2\sqrt{15 m_{eff} E_{eff}} R_{eff}^{1/4} \ln(e_{int})}{3\sqrt{\pi^2 + \ln^2(e_{int})}}\delta^{1/4}, \tag{3.5}$$

where the subscripts i and j represent denote the properties of each of the contacting particles, E is Young's modulus, e_{int} is the intrinsic coefficient of restitution and the effective mass is

$$m_{eff} = \frac{m_i m_j}{m_i + m_j}. \tag{3.6}$$

https://doi.org/10.1017/jfm.2017.642 Published online by Cambridge University Press

A cohesion model that accounts for van der Waals forces is used in this work for the purposes of illustration, although other cohesion models can be used to develop the cohesion-specific closures for the continuum theory. Here, a modified two-scale Rabinovich *et al.* (2000) theory was used to estimate van der Waals forces. This theory accounts for cohesion between all combinations of large- (L) and small- (S) scale roughness on both particles. The magnitude of the force between particles i and j is given by Liu *et al.* (2016*b*),

$$F_{coh}(D > D_{min}) = \frac{A}{6}\left[\frac{R_i R_j}{(R_i + R_j)(D + y_{iL} + y_{jL} + y_{iS} + y_{jS})^2}\right.$$
$$+ \frac{R_i r_{jL}}{(R_i + r_{jL})(D + y_{iL} + y_{iS} + y_{jS})^2}$$
$$+ \frac{R_i r_{jS}}{(R_i + r_{js})(D + y_{iL} + y_{iS})^2} + \frac{r_{iL} R_i}{(r_{iL} + R_j)(D + y_{iS} + y_{jL} + y_{jS})^2}$$
$$+ \frac{r_{iL} r_{jL}}{(r_{iL} + r_{jL})(D + y_{iS} + y_{jS})^2} + \frac{r_{iL} r_{jS}}{(r_{iL} + r_{jS})(D + y_{iS})^2}$$
$$\left. + \frac{r_{iS} R_j}{(r_{iS} + R_j)(D + y_{iL} + y_{jS})^2} + \frac{r_{iS} r_{jL}}{(r_{iL} + r_{jL})(D + y_{jS})^2} + \frac{r_{iS} r_{jS}}{(r_{iS} + r_{jS})D^2}\right], \quad (3.7)$$

$$r_{kl} = \frac{\lambda_{kl}^2}{32 k_1 rms_{kl}}, \quad y_{kl} = k_1 rms_{kl}, \quad (3.8a,b)$$

where λ is the wavelength of the roughness, $k_1 = 1.817$ is a geometric constant, rms_{kl} is the root mean square height of asperities, r_{kl} is the radius of asperities and y_{kl} is the asperity height, with the subscript k taking values of i or j and the subscript l taking values of S or L. Here, A is the Hamaker constant, R is the particle radius, D is the distance between the highest asperity of the two particles and D_{min} is the cutoff distance, frequently taken to be the intermolecular separation distance. When particles are separated by less than the minimum cutoff distance,

$$F_{coh}(D \leqslant D_{min}) = F_{coh}(D_{min}). \quad (3.9)$$

The values of the particle properties for this cohesive model are summarized in table 1. The values used correspond to glass beads, similar to those used in previous experiments (LaMarche *et al.* 2017).

3.2. *Systems examined*

Discrete element method simulations were used both to extract the cohesion-specific quantities ($v_{a,crit}$, $v_{b,crit}$, $d_{V,V'}$ and e_{eff}) and to validate the continuum theory. Since a lightly cohesive system is considered here (only singlets and doublets), only one distribution of daughters (b) is possible (two singlets), thereby precluding the need to determine this quantity. Different systems were utilized for these purposes, as described below.

3.2.1. *Controlled two-particle DEM*

Controlled two-particle DEM simulations were utilized to determine the critical velocity of aggregation for singlet–singlet collisions $v_{a,1,1,crit}$, as needed to evaluate the success factor of aggregation ψ_a (2.11) and the effective coefficient of restitution e_{eff} (2.38). Namely, simulations of two particles colliding at various impact angles

https://doi.org/10.1017/jfm.2017.642 Published online by Cambridge University Press

Parameter	Dimensionless form	Value
Large-scale roughness rms_1	rms_1/d_1	4.17×10^{-2}
Large-scale wavelength λ_1	λ_1/d_1	5.77×10^{-5}
Small-scale roughness rms_2	rms_2/d_1	3.77×10^{-7}
Small-scale wavelength λ_2	λ_2/d_1	3.46×10^{-6}
Cutoff distance D_{min}	D_{min}/d_1	6.25×10^{-6}
Intrinsic (input) coefficient of restitution	e_{int}	0.97
Poisson ratio	ν	0.22
Young's modulus E	Ed_1^3/A	1.05×10^{11}
Domain size $L = W = H$	$L/d_1 = W/d_1 = H/d_1$	13.8
Initial granular temperature (SSF) $T_{s,0}$	$T_{s,0}/(\rho d_1^3 v_{a,crit,1,1}^2)$	42.2
Initial granular temperature (HCS) $T_{s,0}$	$T_{s,0}/(\rho d_1^3 v_{a,crit,1,1}^2)$	21.1
Shear rate (SSF) γ	$\gamma^* = \gamma d_1/v_{a,crit,1,1}$	0–3.04
Solids volume fraction	ε_s	0.05–0.3
DEM time step Δt	$\Delta t(A/(\rho d_1^5))^{1/2}$	1.93×10^{-7}

TABLE 1. The dimensionless input parameters (particle and system) used in the DEM simulations.

and velocities were performed to determine whether aggregation or rebound occurred. This two-particle system was chosen to determine $v_{a,1,1,crit}$ for colliding singlets, as singlet–singlet collisions have limited orientations and the full parameter space is easily covered. (Nonetheless, it should be recalled that the normal critical velocity of aggregation was found to be independent of the collision orientation, as shown in figure 1.)

Controlled DEM simulations were not used to determine the critical velocity of breakage $v_{b,1,2,crit}$, nor the collision cylinder diameter $d_{1,2}$, however, as the parameter space of collisions involving doublets becomes quite large with the inclusion of added parameters – e.g. orientation and rotation speed of the doublet at time of collision (Liu *et al.* 2017). Further, if the simulation is extended to consider collisions with larger agglomerates, additional parameters such as the packing of agglomerate (compact versus loose) and agglomerate shape must be considered. Perhaps more importantly, we found via such controlled DEM simulations that $v_{b,1,2,crit}$ depends on the collision orientation and gives rise to some outlier values. Direct account for the dependence of $v_{b,1,2,crit}$ on the impact orientation is not possible in the continuum framework since this quantity not known *a priori* or solved for. Thus, as a first step, we use a constant mean value of $v_{b,1,2,crit}$ in this work. Moreover, the collision orientations associated with outlier values of $v_{b,1,2,crit}$ observed in controlled DEM simulations were seldom seen to occur in the many-particle flow systems considered here, although they greatly influence the mean critical velocity extracted from a range of collision orientations. Therefore, generally speaking, it is important to determine the critical velocity of breakage, the critical velocity of aggregation for agglomerates, the collision cylinder diameters and the daughter distributions from such many-particle flows, where these outlier collisions are infrequent. In the work described herein, we will use many-particle SSF simulations to determine $v_{b,1,2,crit}$ since shear is often present in practical cohesive flows.

3.2.2. *Simple shear flow*

Simple shear flow was achieved via periodic walls on four sides of the domain. The remaining two opposite sides were simulated using Lees–Edwards boundary

https://doi.org/10.1017/jfm.2017.642 Published online by Cambridge University Press

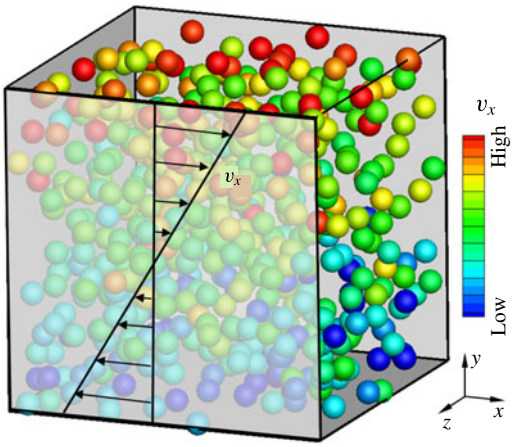


FIGURE 5. (Colour online) Schematic of an SSF system in the DEM. The transparent front pane shows the mean velocity profile.

conditions, which impose a constant velocity gradient (Lees & Edwards 1972), as shown in figure 5. The domain was chosen to have dimensions of $L/d = 13.8$ in order to prevent clustering instabilities (see (Fullmer & Hrenya 2017) for a review), which would cause the system to become inhomogeneous and thus complicate the prediction of the local granular temperatures and success factors. Preliminary simulations of the SSF system indicated that at low initial granular temperatures and/or low shear rates, the system evolves into one large agglomerate. Therefore, the SSF simulations were initialized with a granular temperature much greater than the steady-state value, and using (higher) shear rates that lead to a distribution of agglomerate sizes. Particles were initialized at random locations within the domain, with fluctuating velocities determined by a Maxwellian distribution, where the mean velocity was given by the imposed shear velocity at that location and the variance given by the initial granular temperature. For both the SSF and HCS, replicate DEM simulations with different random seed initial conditions showed little sensitivity in the results explored to the initial conditions. These simulations approached a steady state by $t^* = t(A/(\rho d_1^5))^{1/2} \sim 2$ (where ρ is the particle density, A is the Hamaker constant and d_1 is the diameter of a singlet) and were continued until a dimensionless time of $t^* \sim 10$ in order to collect adequate statistics. Only (statistical) steady-state values were utilized in the analysis of this system.

Simple shear flow simulations were used to determine the critical velocity of breakage $v_{b,1,2,crit}$ between a singlet and a doublet as well as the collision cylinder diameter $d_{1,2}$. More specifically, $v_{b,1,2,crit}$ was determined by extracting the success factor of breakage ψ_b as well as the granular temperature T_s from the DEM simulations, and then calculating the critical velocity of breakage according to (2.12),

$$\Psi_b(1,2) = \int_{v_{b,1,2,crit}}^{\infty} f(v_n)\,\mathrm{d}v_n = \exp\left[\frac{-v_{b,1,2,crit}^2}{2T_s\left[\dfrac{1}{m_1}+\dfrac{3}{m_2 5}\right]}\right], \tag{3.10}$$

where m_1 and m_2 are the masses of singlets and doublets, respectively.

https://doi.org/10.1017/jfm.2017.642 Published online by Cambridge University Press

Simple shear flow simulations were also used to determine the collision cylinder diameter for singlet–doublet collisions $d_{1,2}$ (distance between the centres of the agglomerate and the colliding singlet particles) used in the breakage kernel for doublets (3.10). This parameter is directly related to the projected sweep area of a doublet, and consequently influences the frequency of collisions.

Daughter distributions can be estimated determined from DEM SSF simulations, but are not required for the lightly cohesive system considered here, as the largest agglomerates considered are doublets, which always produce two singlets when broken.

3.2.3. *Homogeneous cooling system*

For the purposes of initial validation studies of the new continuum theory, the HCS was utilized. The HCS was transient, with the state of the system approaching one large agglomerate with a near-zero granular temperature. Periodic walls were utilized on all sides, and the system was initially (approximately) homogeneous, with no net momentum and no external forces. These simulations were arbitrarily initialized with the granular temperature given in table 1. Because the focus here is on validating the approach for a lightly cohesive system where only singlets and doublets are present, simulation results were only considered up to the time when 3 % of the particles were in agglomerates larger than doublets. Moreover, it should be noted that the distribution of collision orientations in the HCS differs from that of SSF, so this system will be used to make a first assessment of the validity of using a mean value of $v_{b,1,2,crit}$ determined from SSF.

3.2.4. *Agglomerate detection and simulation parameters*

Agglomerates in the DEM simulations were detected using a method that records the collision duration between individual particles. Figure 6 demonstrates a steep drop-off in the frequency of collision duration for the SSF systems examined here and outlined in table 1. This drop-off forms a boundary between shorter collisions that correspond to particles rebounding from non-agglomerating collisions, and longer collisions that correspond to particles agglomerating. A critical collision duration of $t^*_{crit} = t_{coll}(A/(\rho d_1^5))^{1/2} \sim 5.7 \times 10^{-5}$ (dashed black line) was chosen for agglomerate detection, as this corresponds to the steep drop-off over a wide range of system parameters. Particles in contact for longer than this critical value were identified as agglomerates. This agglomerate detection algorithm is demonstrated in figure 7. Figure 7(*a*) shows all of the particles in a cohesive DEM SSF. In figure 7(*b*), only the agglomerates detected in figure 7(*a*) are shown.

3.3. *Continuum theory*

The continuum theory, namely the population balance and granular energy balances, was used to predict the number density of particles in singlets (n_1) and doublets (n_2), along with the (statistically steady) granular temperature (T_s) for SSF. The continuum theory was also used to solve for n_1, n_2 and T_s as they evolved in time for the HCS. The initial conditions of the HCS and SSF continuum simulations were identical to those used in the DEM.

Although a polydisperse kinetic theory may be more appropriate for a system with a broad distribution of agglomerate sizes, the focus here is on the closure of the population balance for a lightly cohesive system dominated by singlets and doublets, with mostly singlets (i.e. not a broad distribution of agglomerate sizes). Thus, the

https://doi.org/10.1017/jfm.2017.642 Published online by Cambridge University Press

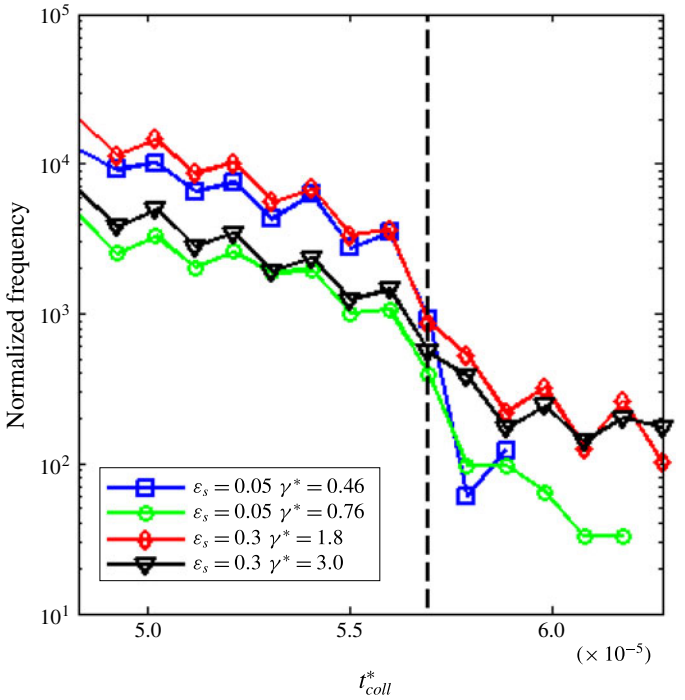


FIGURE 6. (Colour online) Frequency of non-dimensional collision durations ($t^*_{coll} = t_{coll}(A/(\rho d_1^5))^{1/2}$) in a wide range of cohesive DEM SSF simulations. The dashed black line shows the threshold for agglomerate detection. The results are normalized by the number of collisions that occurred in each simulation.

monodisperse kinetic theory given by Garzó & Dufty (1999) was used to provide the closures for the solid stress and the dissipation rate based on a particle size/mass equal to that of a primary particle. It should also be noted that for the SSF and HCS explored here, no slip velocity exists between the different agglomerate sizes (i.e. $|\boldsymbol{u}_V - \boldsymbol{u}_{V'}| = 0$). In other systems where slip does exist between the different agglomerate sizes, a polydisperse kinetic theory that takes into account the effect of the slip on the collision frequency must be used (Garzó *et al.* 2007*a*,*b*; Hrenya 2011). The assumption that a monodisperse kinetic theory is applicable here will be checked later. Further, the granular energy was assumed to be equal for all agglomerate sizes (equipartition of energy), and thus only one granular energy balance was required.

3.3.1. *Simple shear flow*

For a homogeneous SSF system, the population balances (2.1), (2.3), (2.5), (2.7) reduce to

$$0 = -2\beta_{1,1}n_1n_1 + 2\alpha_{1,2}n_1n_2, \tag{3.11}$$

where n_1 and n_2 are the number densities of singlets and doublets, $\beta_{1,1}$ is the aggregation kernel of singlets and $\alpha_{1,2}$ is the breakage kernel of doublets due to collisions with singlets. The granular energy balance reduces to

$$0 = \frac{2}{3n_{particles}}\mu\gamma^2 - \zeta T_s, \tag{3.12}$$

https://doi.org/10.1017/jfm.2017.642 Published online by Cambridge University Press

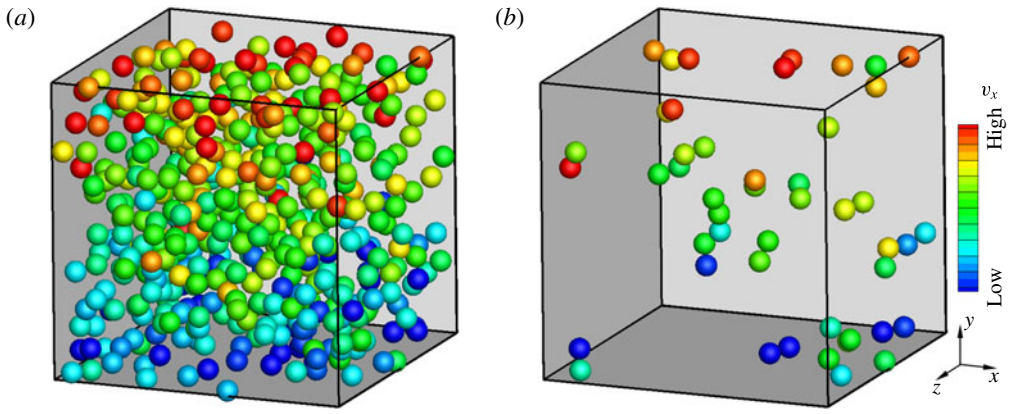


FIGURE 7. (Colour online) (*a*) Snapshot of a cohesive DEM SSF system with all of the particles present ($\varepsilon_s = 0.10$, $\gamma^* \sim 0.90$). (*b*) Snapshot of only the agglomerates detected in (*a*).

where T_s is the granular temperature, μ is the granular shear viscosity, $n_{particles}$ is the total number density of (primary) particles in the system, γ is the shear rate and ζ is the dissipation coefficient. Here, ζ and μ were determined by substituting the mean effective coefficient of restitution ($\langle e_{eff} \rangle$; see (2.38)) in place of the (intrinsic) coefficient of restitution in the constitutive relations given by Garzó & Dufty (1999). The first term on the right-hand side of the equation represents the generation of granular energy due to shear and the second term represents the dissipation of granular energy due to inelastic collisions. It is worthwhile to note that only one-way coupling is present between the population and granular energy balances – i.e. the granular temperature can be solved independently of the population balances, but not vice versa, since $\alpha_{1,2} = f(T_s)$.

Each combination of shear rate and solids volume fraction represents an independent simulation (i.e. each DEM data point (figures 8–13) represents an independent simulation with a different random initial condition). The error bars shown on these figures for the DEM results reflect the standard deviation after steady state is reached. Similarly, a corresponding continuum solution was obtained for each condition simulated via the DEM.

3.3.2. *Homogeneous cooling system*

For the HCS, the population balances are identical to those of SFF, except with time derivative terms included, as the system is transient,

$$\frac{\mathrm{d}n_1}{\mathrm{d}t} = -2\beta_{1,1} n_1 n_1 + 2\alpha_{1,2} n_1 n_2, \tag{3.13}$$

$$\frac{\mathrm{d}n_2}{\mathrm{d}t} = \beta_{1,1} n_1 n_1 - \alpha_{1,2} n_1 n_2. \tag{3.14}$$

In the absence of shear, the granular energy balance further reduces to

$$\frac{\mathrm{d}T_s}{\mathrm{d}t} = -\zeta T_s, \tag{3.15}$$

https://doi.org/10.1017/jfm.2017.642 Published online by Cambridge University Press

where the dissipation of granular energy in time is dictated by inelastic collisions. Similarly to the SSF system, only one-way coupling exists between the granular energy and the population balances for the homogeneous cooling simulations. The population and granular energy balance equations were solved until 3 % of the particles were in agglomerates larger than doublets.

Five independent DEM simulations (with different random initial conditions) were performed for each solids volume fraction in the HCS. The error bars shown in figures 14 and 15 indicate the standard deviation of the DEM results from these five independent simulations. A single continuum solution was found for each solids volume fraction.

3.3.3. *Numerical solution*

Using an in-house MatLab script, an implicit Euler time march was used to solve the transient population and energy balances for the HCS simulations. For the SSF simulations, the transient terms were reintroduced, and the same implicit Euler time march was used to relax the agglomerate size distributions and granular temperatures to the steady-state solutions (i.e. the transient terms approached zero, consistent with (3.11)–(3.12)). For both systems, an adjustable time step was used to overcome initial stiffness in the system. To ensure numerical accuracy, insensitivity to the time step and residual values was confirmed for a few test cases encompassing the parameter space.

4. Results and discussion

4.1. *Extraction of cohesion-specific quantities needed for continuum-theory closures: collision cylinder diameter and critical velocities*

Three quantities were extracted from DEM simulations for use in the continuum theory: the collision cylinder diameter for singlet–doublet collisions, $d_{V,V'}$ (via SSF), the critical velocity of aggregation for singlet–singlet collisions, $v_{a,1,1,crit}$ (via controlled two-particle collisions), and the critical velocity of breakage for singlet–doublet collisions, $v_{b,1,2,crit}$ (via SSF). The results for these cohesion-specific quantities are summarized in table 2. For the lightly cohesive system explored here, doublet–doublet collisions were neglected because the low concentration of doublets led to a very low frequency of doublet–doublet collisions relative to singlet–doublet collisions, thus making the breakage of doublets due to these types of collisions negligible.

The quantity $d_{V,V'}$ was determined by averaging the distance between the centre of the doublet and the centre of the singlet for collisions of singlets and doublets detected in SSF simulations. The quantity $v_{a,1,1,crit}$ was measured using controlled two-particle DEM simulations (see figure 1).

As described in § 3.2.2, $v_{b,1,2,crit}$ was determined from the measured success factors of breakage ψ_b in DEM SSF and using the closure for the success factor of breakage given in (2.12). The value of $v_{b,1,2,crit}$ shows a slight downward trend as the shear rate γ^* increases; see figure 8. A plausible explanation for this observation is the following: as the shear rate increases, agglomerate rotation increases, thus making it easier for agglomerates to break (the rotational motion adds to the normal impact velocity due to translational motion alone). Additional simulations for different values of $v_{b,1,2,crit}$ across the range measured in figure 8 were performed, and $\psi_{b,1,2}$ was found to be insensitive to $v_{b,1,2,crit}$ in this range, so use of a mean value in the continuum theory was deemed to be acceptable.

https://doi.org/10.1017/jfm.2017.642 Published online by Cambridge University Press

Parameter	Symbol	Value
Singlet–doublet collision cylinder diameter	$d_{1,2}/d_1$	1.43
Critical velocity of aggregation between two singlets	$v^*_{a,crit,1,1} = v_{a,crit,1,1}(\rho d_1^3/A)^{1/2}$	95.5
Critical velocity of breakage between singlets and doublets	$v^*_{b,crit,1,2} = v_{b,crit,1,2}(\rho d_1^3/A)^{1/2}$	143

TABLE 2. Cohesion-specific quantities extracted from DEM SSF simulations and used as inputs to continuum SSF and HCS simulations.

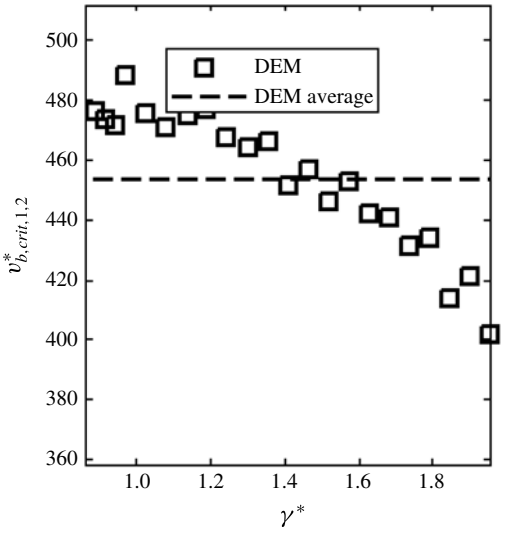


FIGURE 8. Critical velocity of breakage calculated from DEM SSF simulations with $\varepsilon_s = 0.1$ (black points). The dashed line shows the mean value used in continuum theory.

4.2. *Verification and validation of continuum theory: SSF*

Simple shear flow was first used to validate the closure for the success factor of aggregation ψ_a (2.11) and then to validate the closure for $\langle e_{eff} \rangle$ (2.38). As detailed below, the corresponding comparisons with quantities extracted from DEM simulations constitute validation (theory, or closure, accuracy) rather than verification (code accuracy) (Grace & Taghipour 2004) since ψ_a and $\langle e_{eff} \rangle$ depend only on the critical velocity of aggregation $v_{a,1,1,crit}$ determined from DEM simulations of controlled two-particle collisions (rather than SSF). Next, SSF was used for verification (code accuracy) of the aggregation and breakage kernels (2.8)–(2.9). This last comparison is verification (code accuracy) rather than validation (theory accuracy), as the cohesion-specific inputs of the critical velocity of breakage $v_{b,1,2,crit}$ and the collision cylinder diameter $d_{V,V'}$, which were determined from the SSF system, were subsequently used in the continuum-theory predictions for SSF. Further, these latter verifications utilized n_1, n_2 and T_s extracted from the DEM simulations, rather than the predicted values, to ensure that any resulting discrepancies were traceable directly to the aggregation and breakage kernels themselves.

It should be recalled that the success factor $\psi_{a,1,1}$ is used to determine the rate of aggregation in the system (2.3), and is therefore a key quantity for the accurate prediction of the agglomerate size distributions n_1 and n_2. For simple shear flow, $\psi_{a,1,1}$

https://doi.org/10.1017/jfm.2017.642 Published online by Cambridge University Press

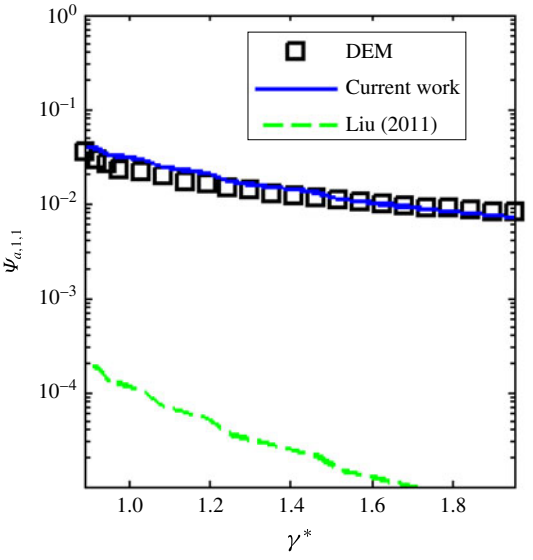


FIGURE 9. (Colour online) Success factor of aggregation for $\varepsilon_s = 0.1$. The solid line shows the prediction by Liu (2011).

was extracted directly from the DEM, and compared with the current theory (2.11), as well as a previous theoretical expression (Liu 2011). Both of these theoretical expressions depend on $v_{a,1,1,crit}$ and T_s. It should be recalled that the value of $v_{a,1,1,crit}$ for these predictions was determined from controlled two-particle DEM simulations, and the value of T_s used in the prediction was extracted directly from the DEM SSF simulations in order to isolate any discrepancies as stemming from the closure for $\psi_{a,1,1}$, rather than uncertainty in T_s. Figure 9 demonstrates that the new theory outlined here correctly predicts the success factor measured via the DEM, whereas the previous theory of Liu (2011) significantly underpredicts $\psi_{a,1,1}$. In the current theory, $\psi_{a,1,1}$ is determined from the distribution of normal impact velocities. The disagreement between $\psi_{a,1,1}$ predicted by the Liu theory (2011) and the DEM simulation results is not surprising since the value of $\psi_{a,1,1}$ in the Liu theory (2011) is determined from the distribution of total impact velocities (including tangential components). These results are consistent with figure 3. That is, at lower impact velocities, the probability of an impact having a given total relative velocity as predicted by the Liu theory (2011) is much smaller than the probability of a collision having the same given normal relative impact velocity as predicted by the current theory. Integration of these impact velocity distributions from 0 to a constant $v_{a,1,1,crit}$ to determine $\psi_{a,1,1}$ (2.11) causes the Liu theory (2011) to underpredict $\psi_{a,1,1}$, as evidenced in figure 9. It should also be noted that for the limiting case of aggregation between singlets, the prediction of $\psi_{a,1,1}$ given by the current model is consistent with the ratio of the frequency of collisions that successfully result in agglomeration to the total collision frequency predicted by Murphy & Subramaniam (2015).

Another closure that can be validated directly via SSF simulations is the kinetic-theory treatment involving $\langle e_{eff} \rangle$. For SSF, the momentum balances are solved identically such that only the energy balance and population balance require solution. It should be recalled that the granular energy balance has one-way coupling with the population balance, such that the granular energy balance affects the population

https://doi.org/10.1017/jfm.2017.642 Published online by Cambridge University Press

balance, but not vice versa. Therefore, the granular energy balance can be solved in isolation for T_s, and any discrepancies between the predicted value and that extracted from the DEM will arise from the kinetic-theory treatment itself (i.e. $\langle e_{eff} \rangle$), and not due to the new closures in the population balance. A comparison between the T_s measured in the DEM and that predicted by the granular energy balance is given in figure 10. The kinetic theory for a non-cohesive system (using the intrinsic property for the coefficient of restitution e_{int} in the dissipation and shear viscosity closures in the granular energy balance (3.14)) is included for comparison with the current (cohesive) theory and DEM simulations. The kinetic theory using e_{int} gives an overestimation of the granular temperature compared with when $\langle e_{eff} \rangle$ is used. The excellent agreement between the DEM results and the kinetic-theory treatment using $\langle e_{eff} \rangle$ provides initial validation for this approach, and also provides support for the monodisperse assumption. Further, this approach gives an excellent prediction of the T_s for a system outside of that explored by Murphy & Subramaniam (2015), which included the effect of e_{eff} (rather than $\langle e_{eff} \rangle$ used here) in the dissipation term only, and was thus restricted to the HCS. Further, the approach used by Murphy & Subramaniam (2015) does not include the shear term (i.e. granular shear viscosity μ, which also depends on e_{eff}) included here.

Above, the closures of the new continuum theory that can be validated using SSF (ψ_a and $\langle e_{eff} \rangle$) are compared successfully with the DEM simulations (theory accuracy); we will now turn our attention to the remaining closures for which verification (code accuracy) can be carried out in SSF, and then move on to the HCS for validation of the same quantities. In particular, for verification purposes, the fraction of particles in doublets ($2n_2/n_{particles}$) predicted by the continuum theory (solution of both the kinetic theory and population balances) for SSF is compared with the DEM results. This comparison is verification since the critical velocity of breakage $v_{b,1,2,crit}$ was determined from the SSF DEM simulations, and this value is then used in the calculation of the fraction of particles in doublets (2.1). The resulting comparisons are shown in figure 11 for a range of concentrations and shear rates. The DEM simulations display a trend of a decreasing fraction of particles in doublets with an increasing shear rate. The same behaviour is captured by the continuum theory. This behaviour is expected, as an increased shear rate leads to an increased (steady state) T_s. An increased T_s (i.e. impact velocity) decreases the likelihood of agglomeration ($\psi_{a,1,1}$) and increases the likelihood of breakage ($\psi_{b,1,2}$), leading to less aggregation and more breakage, and thus fewer doublets.

Quantitatively, a non-systematic deviation exists between the fraction of particles in doublets observed in the DEM and the continuum-theory prediction (figure 11). More specifically, the continuum theory overpredicts the amount of aggregation in some cases (for all shear rates for $\varepsilon_s = 0.05$, for most shear rates at $\varepsilon_s = 0.1$–0.2) and underpredicts for other conditions (the lowest shear rates at $\varepsilon_s = 0.1$–0.25 and for all shear rates at $\varepsilon_s = 0.3$). To identify the source of this deviation, the individual terms in the population balance are considered. In particular, the success factors of aggregation and breakage, the collision frequencies of singlet–singlet and singlet–doublet collisions, and the aggregation and breakage rates are considered individually in figure 12 for the case of $\varepsilon_s = 0.1$. Namely, the product of the success factors (a,d) with the collision frequency (b,e) gives the rates of aggregation and breakage (c,f). Panels (a–c) represent singlet–singlet collisions and (d–f) represent singlet–doublet collisions.

The results for the different terms in the population balance shown in figure 12 explain the overprediction of the fraction of particles in doublets observed in figure 11

https://doi.org/10.1017/jfm.2017.642 Published online by Cambridge University Press

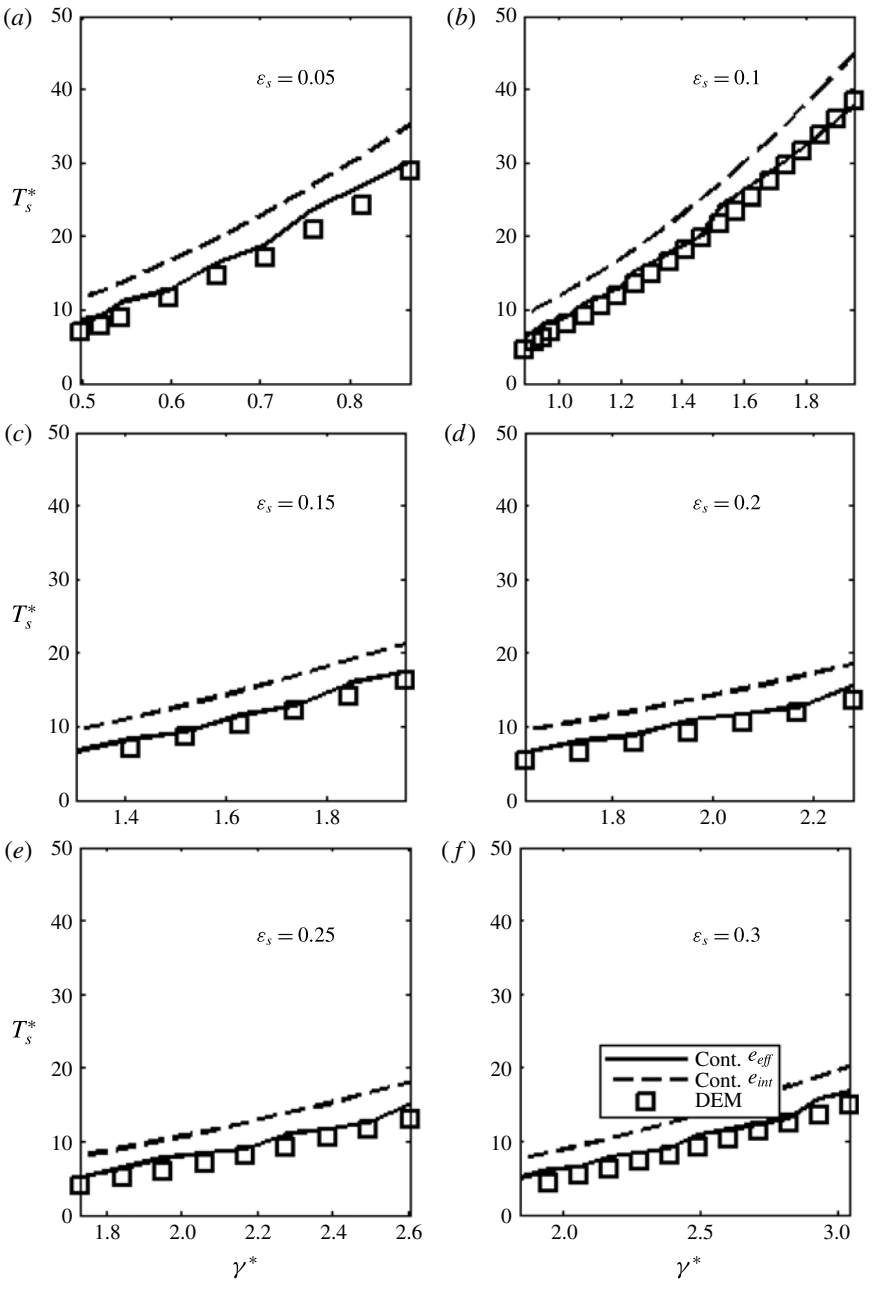


FIGURE 10. Comparison of the non-dimensional granular temperature ($T_s^* = T_s/(\rho d_1^3 v_{a,1,1,crit}^2)$) predicted in SSF by the continuum theory and the DEM for various solids volume fractions and shear rates. The continuum predictions are given by solid lines. The dashed line corresponds to a simulation using the intrinsic, rather than effective, coefficient of restitution. Points represent DEM data.

for $\varepsilon_s = 0.1$. More specifically, figure 12(*a*) demonstrates that the continuum theory overpredicts the success factor $\psi_{a,1,1}$ (except at shear rates greater than $\gamma^* \sim 1.6$) and consequently the singlet–singlet aggregation rate in figure 12(*c*). Further, the

https://doi.org/10.1017/jfm.2017.642 Published online by Cambridge University Press

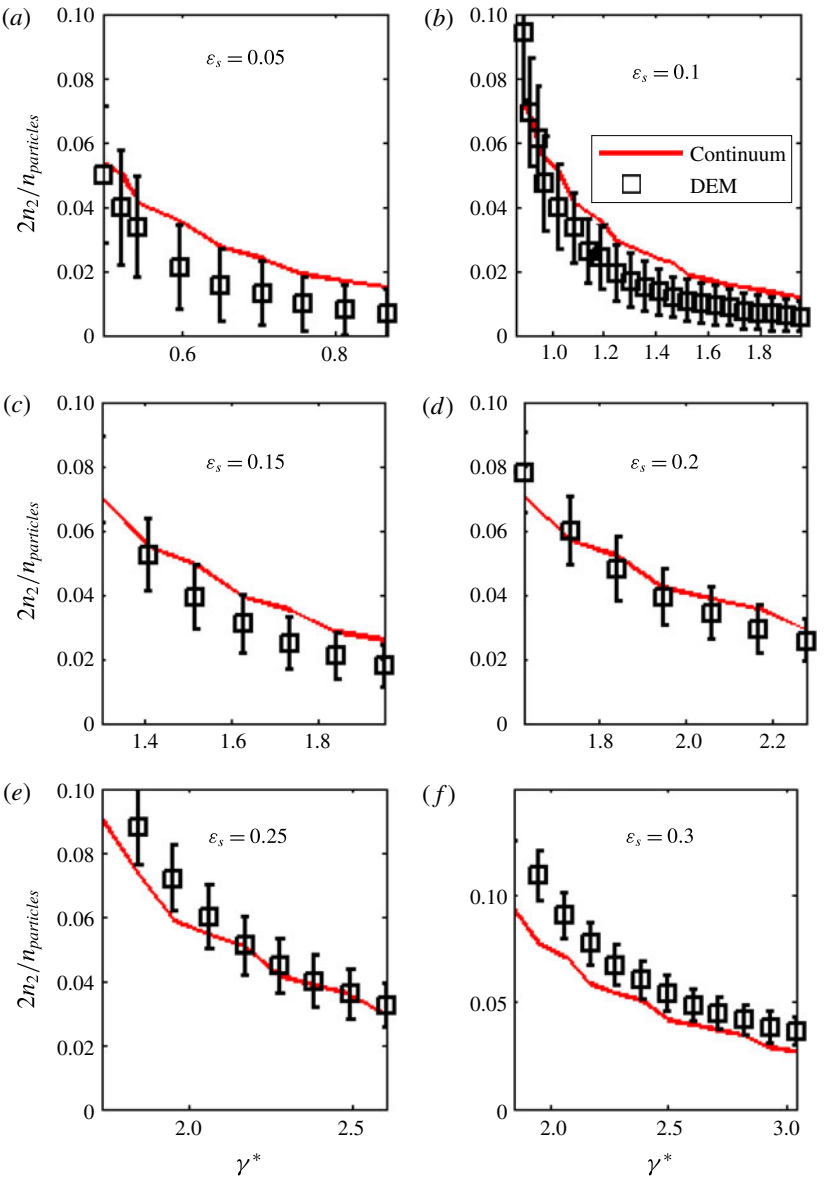


FIGURE 11. (Colour online) Comparison of the fraction of particles in doublets predicted in SSF by the continuum theory (solid lines) and the DEM (points) for various solids volume fractions and shear rates. The error bars show the standard deviation of the fraction of particles at incremental times after steady state was reached for one simulation.

continuum theory slightly underpredicts the collision frequency of singlet–doublet collisions $N_{1,2}$ (figure 12*e*) for all shear rates, which causes a small underprediction in the breakage rate of doublets (figure 12*f*). Collectively, these effects lead to an overprediction of particles in doublets for higher shear rates (figure 11*b*), which explains the deviation between the continuum theory and the DEM observed for shear rates greater than $\gamma^* \sim 0.98$ in figure 11(*b*). In figure 11(*b*), however, the

https://doi.org/10.1017/jfm.2017.642 Published online by Cambridge University Press

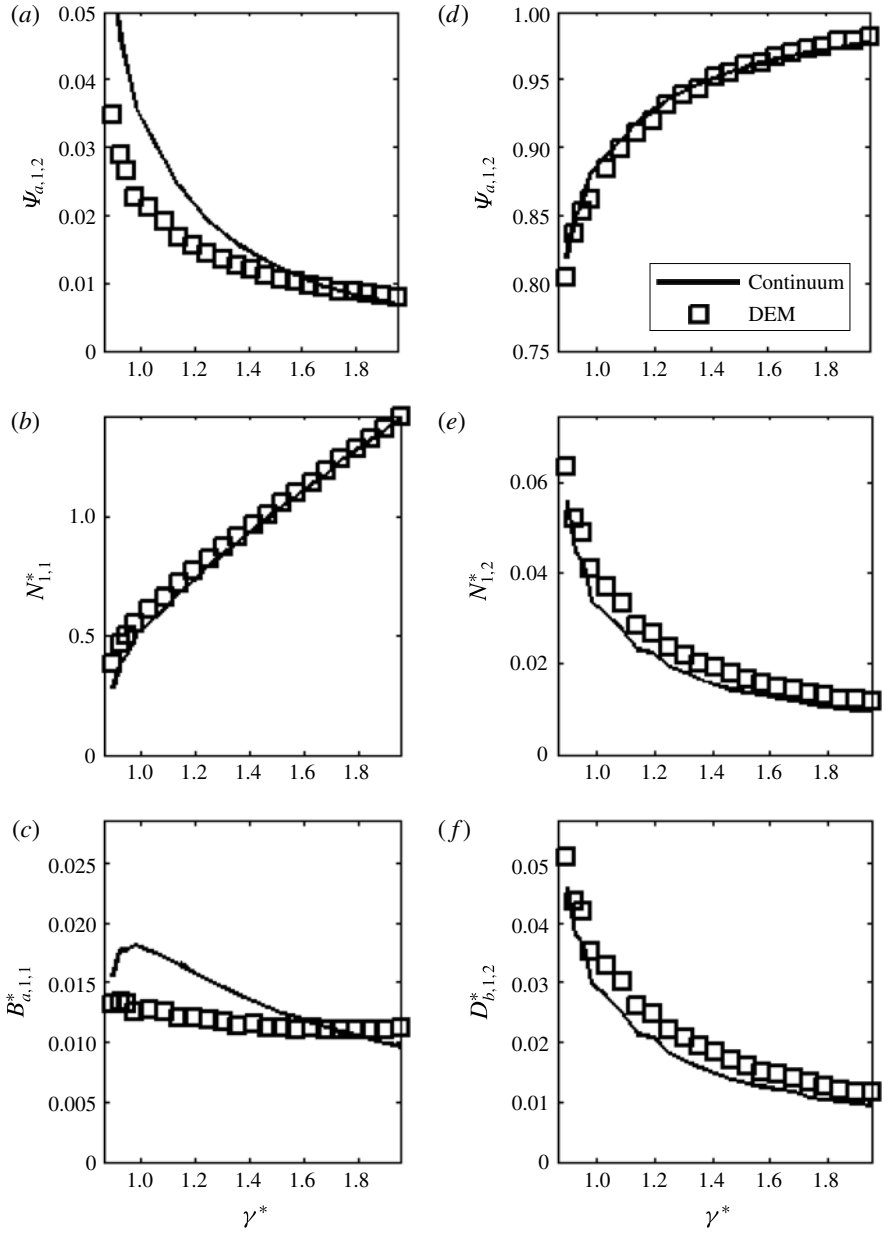


FIGURE 12. Terms associated with aggregation and breakage rates for $\varepsilon_s = 0.1$ for (*a–c*) singlet–singlet interactions and (*d–f*) singlet–doublet interactions. Collision frequencies and aggregation and breakage rates are non-dimensionalized by multiplying by $d_1^4/v_{a,1,1,crit}$.

continuum theory appears to accurately predict the fraction of particles in doublets at the lowest shear rates of $\gamma^* \sim 0.87$–0.98. One possible explanation for the absence of the expected mismatch is that the continuum theory is missing a sink of doublets, which would counteract the overprediction expected from figure 12(*c*,*f*).

https://doi.org/10.1017/jfm.2017.642 Published online by Cambridge University Press

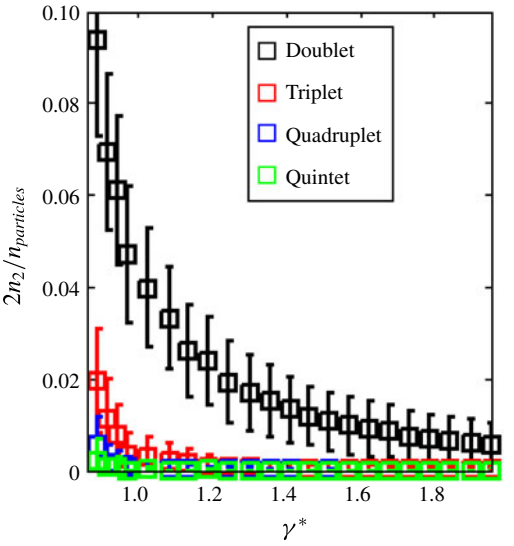


FIGURE 13. (Colour online) Distribution of larger agglomerates in DEM SSF for $\varepsilon_s = 0.1$. The error bars show the standard deviation of the fraction of particles in agglomerates for different times after steady state was reached in one simulation.

To explain the discrepancy noted above, it is hypothesized that the birth of larger agglomerates (larger than doublets) due to aggregation may provide the missing net sink of doublets. Indeed, figure 13 indicates that larger agglomerates are present, especially at lower shear rates. More specifically, the doublet fraction in the DEM was observed to remain at a statistical steady state in time, requiring that the net source of doublets be zero. However, calculations confirm that an estimate of the net source of doublets observed in the DEM ($\varepsilon_s = 0.1$), based only on the aggregation rate of singlets less the breakage rate of doublets, is indeed non-zero for $\gamma^* < 0.2$ (not shown for the sake of brevity). Therefore, agglomerates involving three particles or more, which were ignored in the application of the continuum theory to these lightly cohesive systems, are needed for the net source of doublets at steady state to equal zero at such low shear rates. Moreover, the results shown in figures 9–11 have better agreement at higher shear rates (higher T_s) due to the lack of larger agglomerates (figure 13). Accordingly, for purposes of verification, attention should be restricted to the higher shear rates of $\gamma^* > 0.98$, since the continuum theory was applied assuming that only singlets and doublets are present (i.e. population balances for n_3, etc., which are beyond the scope of this work, were not included). Within this range, the results in figures 11 and 12 provide sound verification of the aggregation and breakage kernels contained in the new continuum theory.

4.3. *Validation of continuum theory: HCS*

As detailed above, SSF provides a simple steady-state validation of the use of $\langle e_{eff} \rangle$ in kinetic-theory closures as well as the success factor ψ_a appearing in the population balance. The HCS, by contrast, provides a simple transient validation case for the terms mentioned above, as well as the aggregation and breakage kernels (β and α respectively) in the population balance. First, the granular temperature T_s predicted by the continuum theory for the HCS is compared with T_s measured in the DEM,

https://doi.org/10.1017/jfm.2017.642 Published online by Cambridge University Press

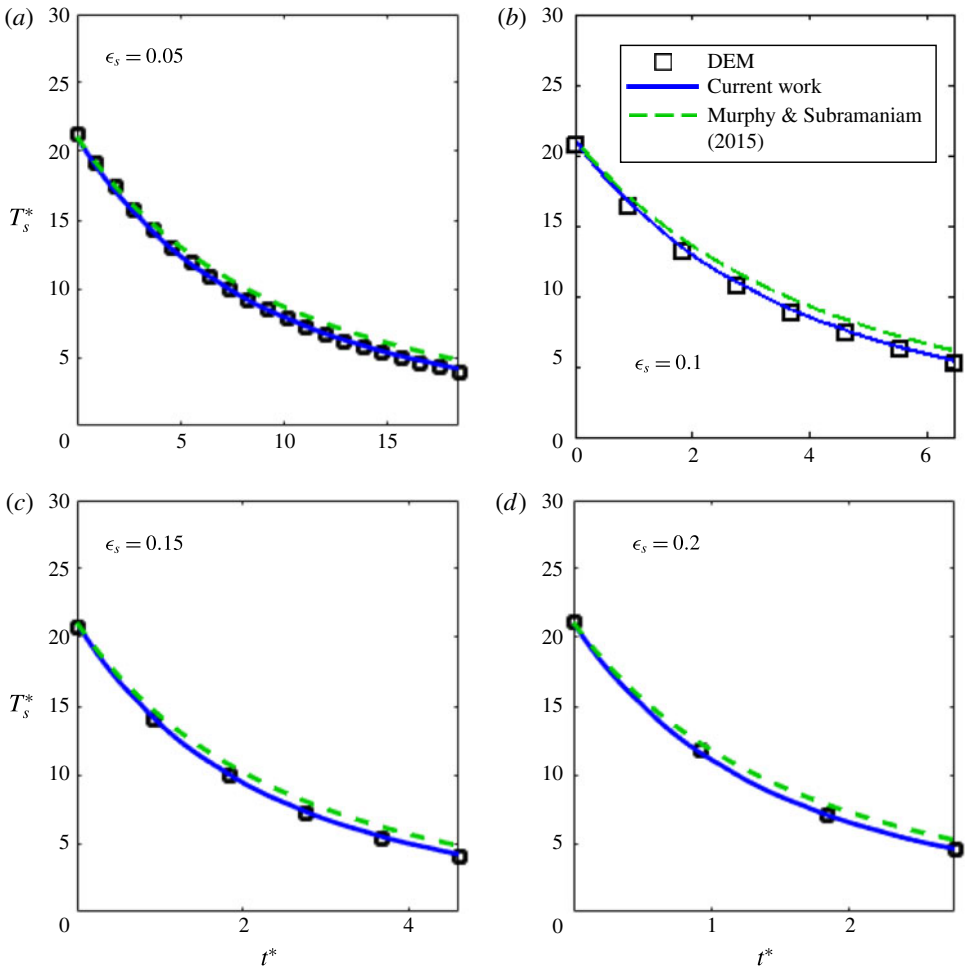


FIGURE 14. (Colour online) Granular temperature in the HCS predicted by the current work and Murphy & Subramaniam (2015) compared with the DEM.

as well as the prediction given by Murphy & Subramaniam (2015), in figure 14. The results are all in very good agreement, providing initial validation of the kinetic-theory treatment using $\langle e_{eff} \rangle$. The slight deviation of the granular temperature predicted by Murphy & Subramaniam's (2015) theory from the DEM results and the new theory presented here is associated with the fourth moment of $f^{(0)}$, or equivalently the c^* constant in the theory of Garzó & Dufty (1999). This constant takes into account the deviation of elastic particles from an inelastic gas. Such effects are inherent in the DEM simulations, and are taken into account in the new theory through the use of Garzó and Dufty's constitutive relations (1999), but were not taken into account in the work of Murphy & Subramaniam (2015).

It should be noted that the model given by Murphy & Subramaniam (2015) does not incorporate the effects of e_{eff} into the terms other than the dissipation rate of granular energy, and therefore can only be applied to the HCS. Again, it should be noted that there is one-way coupling between the granular energy balance and the population balance, such that the granular energy balance affects the population balance, but

https://doi.org/10.1017/jfm.2017.642 Published online by Cambridge University Press

not vice versa. Accordingly, the excellent predictions for T_s resulting from the $\langle e_{eff} \rangle$ treatment indicate that any potential discrepancy in predictions for n_1 and n_2 can be traced to the population balance, and do not stem from the kinetic-theory treatment.

Finally, the fraction of particles in agglomerates in the HCS predicted by the continuum theory is compared with the DEM data in figure 15. The fraction of particles in agglomerates is observed to increase in time. More specifically, as time increases, T_s decreases due to dissipation from inelastic collisions (figure 14). As T_s decreases, the success factor of agglomeration ψ_a increases (due to lower impact velocities) while the collision frequency $N_{1,1}$ decreases. The former leads to an increase in doublet formation, while the latter has the opposite effect. Thus, at earlier times when T_s is high, the higher rate of doublet formation can be traced to the high collision frequency despite the lower success factor. As T_s decreases with time, the reduced collision frequency leads to a lower rate of doublet formation (smaller slope), although doublet formation still increases with time since the likelihood of agglomeration is greater for smaller impact velocities. The continuum theory captures the inflection at $t^* \sim 0.2$–0.5 caused by these competing mechanisms of aggregation.

5. Closing remarks

In this work, the effects of short-range attractive forces (cohesion) on rapid solid-particle flows were fundamentally incorporated into a continuum framework that comprised the population balance as well as the kinetic-theory-based balances for momentum and granular energy. Specifically, novel expressions for the aggregation and breakage rates used in the population balance were derived. Similarly to previous works, these rates are given by the product of the collision frequency and the fraction of collisions resulting in aggregation and breakage events (i.e. success factors). Unlike previous works, the success factors of aggregation and breakage were found by integrating the derived distribution of normal impact velocities over the range of impact velocities that result in aggregation and breakage. The normal impact velocity (a quantity specific to an individual collision) distribution was related to the granular temperature (continuum quantity) for use in the continuum theory. Cohesion was further accounted for in the kinetic theory via a physically based 'effective' coefficient of restitution, which also depends on the impact velocity or, equivalently, the granular temperature.

The aforementioned derivation resulted in a general form of the continuum balances, namely one that is independent of the mechanism of cohesion. To apply these equations to a specific type of cohesion, several quantities that are specific to the type of cohesion (van der Waals, capillary forces, etc.) and the corresponding particles (Hamaker constant, surface tension, etc.) must be specified. In particular, the cohesion-specific quantities needed for a fully specified system of equations are the critical velocities of aggregation and breakage ($v_{a,V,V',crit}$ and $v_{b,V,V',crit}$), the collision cylinder diameters ($d_{V,V'}$), the daughter distribution (b) and e_{eff}. For a given type of cohesion, experiments and/or theoretical estimates (e.g. Donahue *et al.* 2012; Gollwitzer *et al.* 2012) can be used to determine the cohesion-specific quantities. These values can then be used in the continuum theory developed here. As an illustrative example of how to obtain these cohesion-specific inputs, we considered granular flows (no interstitial fluid) with particles experiencing light van der Waals cohesion. Consequently, the systems were dominated by mostly singlets and some doublets, allowing for the monodisperse assumption to be used in the kinetic-theory-based balances.

https://doi.org/10.1017/jfm.2017.642 Published online by Cambridge University Press

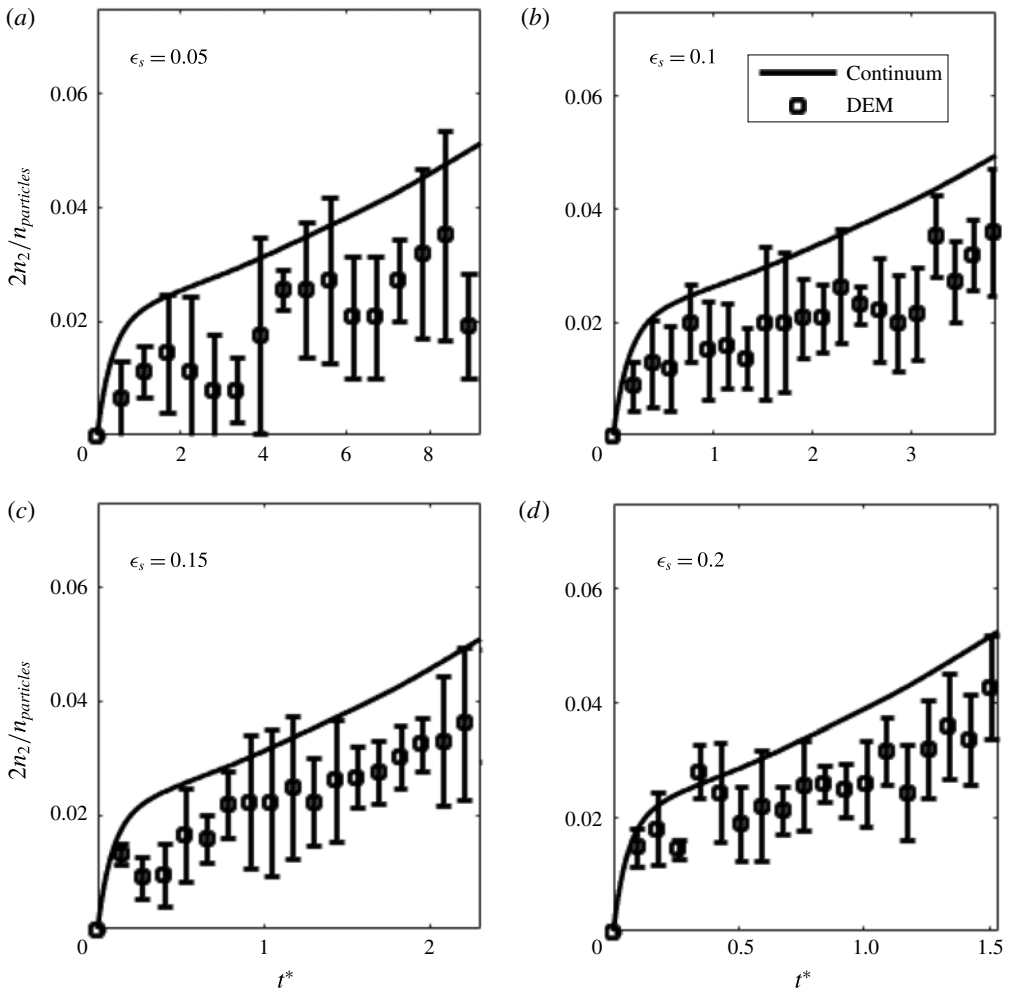


FIGURE 15. Fraction of particles in doublets for the HCS with non-dimensional time, $t^* = tv_{a,crit,1,1}/d_1$. The lines show the continuum prediction, the points show the DEM results and the error bars show the standard deviation of five repeats.

In this work, the cohesion-specific quantities were extracted from DEM simulations. Namely, $v_{a,1,1,crit}$ was determined using controlled two-particle DEM simulations, while a new methodology was introduced to determine $v_{b,1,2,crit}$ and $d_{1,2}$ via many-particle DEM simulations of simple shear flow. The daughter distribution b was not needed for these lightly cohesive systems, as doublets only form one size of daughters when they break (singlets).

The extracted cohesion-specific quantities were then used as inputs to the continuum theory derived here and the results were compared with DEM simulations of two simple cases, namely SSF and the HCS. Comparisons between continuum predictions and DEM simulations for several of the closures themselves (e.g. success factor of agglomeration ψ_a), as well as the continuum variables n_1, n_2 and T_s, are excellent, providing initial validation of the new approach to closing the population and kinetic-theory balances described here.

https://doi.org/10.1017/jfm.2017.642 Published online by Cambridge University Press

The results presented here are encouraging, and warrant further exploration and testing of the new continuum theory for cohesive-particle flows. That is, the continuum theory can be extended to other mechanisms and/or higher levels of cohesion in a straightforward manner. Future work is needed to explore the use of the continuum theory with these other sources of cohesion (e.g. liquid bridging). Moreover, for more cohesive particles, larger agglomerates form, which necessitates the determination of their critical velocities of agglomeration and breakage ($v_{a,crit}$ and $v_{b,crit}$ respectively), the collision cylinder diameters ($d_{V,V'}$) and daughter distributions (b) for additional agglomerate sizes. Finally, this continuum framework should be explored in the context of multiphase flows, where the role of the fluid phase cannot be ignored, such as in fluidized beds or pneumatic conveyors.

Acknowledgement

We would like to acknowledge the generous financial support provided by the Dow Corning Corporation.

REFERENCES

ABBASFARD, H., EVANS, G. & MORENO-ATANASIO, R. 2016 Effect of van der Waals force cut-off distance on adhesive collision parameters in DEM simulation. *Powder Technol.* **299**, 9–18.

ANAND, A., CURTIS, J. S., WASSGREN, C. R., HANCOCK, B. C. & KETTERHAGEN, W. R. 2009 Predicting discharge dynamics of wet cohesive particles from a rectangular hopper using the discrete element method (DEM). *Chem. Engng Sci.* **64** (24), 5268–5275.

ANTYPOV, D. & ELLIOTT, J. A. 2011 On an analytical solution for the damped Hertzian spring. *Europhys. Lett.* **94** (5), 50004.

ARASTOOPOUR, H. & KIM, H. 2002 Extension of kinetic theory to cohesive particle flow. *Powder Technol.* **122** (1), 83–94.

BRAUMANN, A., KRAFT, M. & MORT, P. R. 2010 Parameter estimation in a multidimensional granulation model. *Powder Technol.* **197** (3), 196–210.

BRILLIANTOV, N. V. & PÖSCHEL, T. 2010 *Kinetic Theory of Granular Gases*. Oxford University Press.

BRYAN, J. E. & ROBER PFEFFER, G. T. 1991 A microlevel-based characterization of granular phenomena. *Powder Technol.* **65**, 257–272.

CAHYADI, A., NEUMAYER, A. H., HRENYA, C. M., COCCO, R. A. & CHEW, J. W. 2015 Comparative study of transport disengaging height (TDH) correlations in gas–solid fluidization. *Powder Technol.* **275**, 220–238.

CALVERT, G., GHADIRI, M. & TWEEDIE, R. 2009 Aerodynamic dispersion of cohesive powders: a review of understanding and technology. *Adv. Powder Technol.* **20** (1), 4–16.

CAMERON, I. T., WANG, F. Y., IMMANUEL, C. D. & STEPANEK, F. 2005 Process systems modelling and applications in granulation: a review. *Chem. Engng Sci.* **60** (14), 3723–3750.

CASTELLANOS, A. 2005 The relationship between attractive interparticle forces and bulk behaviour in dry and uncharged fine powders. *Adv. Phys.* **54** (4), 263–376.

CHAUDHURI, B., MEHROTRA, A., MUZZIO, F. J. & TOMASSONE, M. S. 2006 Cohesive effects in powder mixing in a tumbling blender. *Powder Technol.* **165** (2), 105–114.

CHEW, J. W., CAHYADI, A., HRENYA, C. M., KARRI, R. & COCCO, R. A. 2015 Review of entrainment correlations in gas–solid fluidization. *Chem. Engng J.* **260**, 152–171.

COCCO, R. A., FULLMER, W. D., LIU, P. & HRENYA, C. M. 2017 CFD–DEM: modeling the small to understand the large. *Chem. Engng Prog.* **113** (9), 38–45.

COSTA, A., FOLCH, A. & MACEDONIO, G. 2010 A model for wet aggregation of ash particles in volcanic plumes and clouds: 1. Theoretical formulation. *J. Geophys. Res.* **115**, B9.

DAVIS, R. H., RAGER, D. A. & GOOD, B. T. 2002 Elastohydrodynamic rebound of spheres from coated surfaces. *J. Fluid Mech.* **468**, 107–119.

https://doi.org/10.1017/jfm.2017.642 Published online by Cambridge University Press

DAVIS, R. H., SERAYSSOL, J.-M. & HINCH, E. J. 1986 The elastohydrodynamic collision of two spheres. *J. Fluid Mech.* **163** (-1), 479–497.

DONAHUE, C. M., DAVIS, R. H., KANTAK, A. A. & HRENYA, C. M. 2012 Mechanisms for agglomeration and deagglomeration following oblique collisions of wet particles. *Phys. Rev.* E **86** (2).

DONAHUE, C. M., HRENYA, C. M., DAVIS, R. H., NAKAGAWA, K. J., ZELINSKAYA, A. P. & JOSEPH, G. G. 2010 Stokes' cradle: normal three-body collisions between wetted particles. *J. Fluid Mech.* **650**, 479–504.

FADDA, S., CINCOTTI, A., CONCAS, A., PISU, M. & CAO, G. 2009 Modelling breakage and reagglomeration during fine dry grinding in ball milling devices. *Powder Technol.* **194** (3), 207–216.

FAN, R., MARCHISIO, D. L. & FOX, R. O. 2004 Application of the direct quadrature method of moments to polydisperse gas–solid fluidized beds. *Powder Technol.* **139** (1), 7–20.

FIGUEROA, I., LI, H. & MCCARTHY, J. 2009 Predicting the impact of adhesive forces on particle mixing and segregation. *Powder Technol.* **195** (3), 203–212.

FOX, R. O. 2014 On multiphase turbulence models for collisional fluid–particle flows. *J. Fluid Mech.* **742**, 368–424.

FULLMER, W. D. & HRENYA, C. M. 2017 The clustering instability in rapid granular and gas–solid flows. *Annu. Rev. Fluid Mech.* **49** (1).

GALVIN, J. E. & BENYAHIA, S. 2014 The effect of cohesive forces on the fluidization of aeratable powders. *AIChE J.* **60** (2), 473–484.

GANTT, J. A. & GATZKE, E. P. 2006 A stochastic technique for multidimensional granulation modeling. *AIChE J.* **52** (9), 3067–3077.

GARZÓ, V. & DUFTY, J. W. 1999 Dense fluid transport for inelastic hard spheres. *Phys. Rev.* E **59** (5), 5895–5911.

GARZÓ, V., DUFTY, J. W. & HRENYA, C. M. 2007*a* Enskog theory for polydisperse granular mixtures. I. Navier–Stokes order transport. *Phys. Rev.* E **76** (3).

GARZÓ, V., HRENYA, C. M. & DUFTY, J. W. 2007*b* Enskog theory for polydisperse granular mixtures. II. Sonine polynomial approximation. *Phys. Rev.* E **76** (3).

GELDART, D., HARNBY, W. & WONG, A. C. 1984 Fluidization of cohesive powders. *Powder Technol.* **37**, 25–37.

GIDASPOW, D. 1994 *Multiphase Flow and Fluidization: Continuum and Kinetic Theory Descriptions*. Academic.

GOLDHIRSCH, I. 2003 Rapid granular flows. *Annu. Rev. Fluid Mech.* **35** (1), 267–293.

GOLDSCHMIDT, M. J. V. 2001 *Hydrodynamic Modelling of Fluidised Bed Spray Granulation*. Twente.

GOLLWITZER, F., REHBERG, I., KRUELLE, C. A. & HUANG, K. 2012 Coefficient of restitution for wet particles. *Phys. Rev.* E **86** (1).

GRACE, J. R. & TAGHIPOUR, F. 2004 Verification and validation of CFD models and dynamic similarity for fluidized beds. *Powder Technol.* **139** (2), 99–110.

HAMAKER, H. C. 1937 The London–van der Waals attraction between spherical particles. *Physica* **4** (10), 1058–1072.

HENTHORNE, K. & HRENYA, C. 2012 Particle cohesion. In *Particle Theory and Applications*. CRC Press.

HOU, Q. F., ZHOU, Z. Y. & YU, A. B. 2012 Micromechanical modeling and analysis of different flow regimes in gas fluidization. *Chem. Engng Sci.* **84**, 449–468.

HRENYA, C. M. 2011 Kinetic theory for granular materials: polydispersity. In *Computational Gas–Solids Flows and Reacting Systems: Theory, Methods and Practice*, pp. 102–127. IGI Global.

JACKSON, R. 2000 *The Dynamics of Fluidized Particles*. Cambridge University Press.

KAFUI, K. D. & THORNTON, C. 2000 Numerical simulations of impact breakage of a spherical crystalline agglomerate. *Powder Technol.* **109**, 113–132.

KANTAK, A. A., HRENYA, C. M. & DAVIS, R. H. 2009 Initial rates of aggregation for dilute, granular flows of wet particles. *Phys. Fluids* **21** (2), 023301.

https://doi.org/10.1017/jfm.2017.642 Published online by Cambridge University Press

LaMarche, C. Q., Leadley, S., Liu, P., Kellogg, K. M. & Hrenya, C. M. 2017 Method of quantifying surface roughness for accurate adhesive force predictions. *Chem. Engng Sci.* **158**, 140–153.

Le, P. K., Avontuur, P., Hounslow, M. J. & Salman, A. D. 2009 The kinetics of the granulation process: right from the early stages. *Powder Technol.* **189** (2), 149–157.

Lees, A. W. & Edwards, S. F. 1972 The computer study of transport processes under extreme conditions. *J. Phys. C: Solid State Phys.* **5**, 1921–1929.

Lian, G., Thornton, C. & Adams, M. J. 1998 Discrete particle simulation of agglomerate impact coalescence. *Chem. Engng Sci.* **53** (19), 3381–3391.

Liu, L. 2011 Kinetic theory of aggregation in granular flow. *AIChE J.* **57** (12), 3331–3343.

Liu, P., Kellogg, K. M., LaMarche, C. Q. & Hrenya, C. M. 2017 Dynamics of singlet–doublet collisions of cohesive particles. *Chem. Engng J.* **324**, 380–391.

Liu, P., LaMarche, C. Q., Kellogg, K. M., Leadley, S. & Hrenya, C. M. 2016*a* Cohesive grains: bridging microlevel measurements to macrolevel flow behavior via surface roughness. *AIChE J.* **62** (10), 3529–3537.

Liu, P., LaMarche, C. Q., Kellogg, K. M. & Hrenya, C. M. 2016*b* Fine-particle defluidization: interaction between cohesion, Young's modulus and static bed height. *Chem. Engng Sci.* **145**, 266–278.

Liu, D., van Wachem, B. G. M., Mudde, R. F., Chen, X. & van Ommen, J. R. 2016*c* An adhesive CFD–DEM model for simulating nanoparticle agglomerate fluidization. *AIChE J.* **62** (7), 2259–2270.

Mansoori, G. A. 1971 Equilibrium thermodynamic properties of the mixture of hard spheres. *J. Chem. Phys.* **54** (4), 1523.

Mikami, T., Kamiya, H. & Horio, M. 1998 Numerical simulation of cohesive powder behavior in a fluidized bed. *Chem. Engng Sci.* **53** (10), 1927–1940.

Mitrano, P. P., Zenk, J. R., Benyahia, S., Galvin, J. E., Dahl, S. R. & Hrenya, C. M. 2013 Kinetic-theory predictions of clustering instabilities in granular flows: beyond the small-Knudsen-number regime. *J. Fluid Mech.* **738**.

Motlagh, A. H. A., Grace, J. R., Salcudean, M. & Hrenya, C. M. 2014 New structure-based model for Eulerian simulation of hydrodynamics in gas–solid fluidized beds of Geldart group 'A' particles. *Chem. Engng Sci.* **120**, 22–36.

Murphy, E. & Subramaniam, S. 2015 Freely cooling granular gases with short-ranged attractive potentials. *Phys. Fluids* **27** (4), 043301.

Murphy, E. & Subramaniam, S. 2017 Binary collision outcomes for inelastic soft-sphere models with cohesion. *Powder Technol.* **305**, 462–476.

Pannala, S., Syamlal, M. & O'Brien, T. J. 2011 *Computational Gas–Solid Flows and Reacting Systems: Theory, Methods and Practice*. IGI Global.

Rabinovich, Y. I., Adler, J. J., Ata, A., Singh, R. K. & Moudgil, B. M. 2000 Adhesion 1199 between nanoscale rough surfaces. *J. Colloid Interface Sci.* **232** (1), 1016.

Rabinovich, Y. I., Adler, J. J., Ata, A., Singh, R. K. & Moudgil, B. M. 2000 Adhesion between nanoscale rough surfaces. *J. Colloid Interface Sci.* **232** (1), 10–16.

Ramachandran, R., Immanuel, C. D., Stepanek, F., Litster, J. D. & Doyle, F. J. 2009 A mechanistic model for breakage in population balances of granulation: theoretical kernel development and experimental validation. *Chem. Engng Res. Des.* **87** (4), 598–614.

Ramkrishna, D. 2000 *Population Balances: Theory and Applications to Particulate Systems in Engineering*. Academic.

Ringl, C., Bringa, E. M., Bertoldi, D. S. & Urbassek, H. M. 2012 Collisions of porous clusters: a granular-mechanics study of compaction and fragmentation. *Astrophys. J.* **752** (2), 151.

Sela, N. & Goldhirsch, I. 1998 Hydrodynamic equations for rapid flows of smooth inelastic spheres, to Burnett order. *J. Fluid Mech.* **361**, 41–74.

Sen, M. & Ramachandran, R. 2013 A multi-dimensional population balance model approach to continuous powder mixing processes. *Adv. Powder Technol.* **24** (1), 51–59.

Seville, J., Willett, C. & Knight, P. 2000 Interparticle forces in fluidisation: a review. *Powder Technol.* **133**, 261–268.

https://doi.org/10.1017/jfm.2017.642 Published online by Cambridge University Press

TAN, H. S., GOLDSCHMIDT, M. J. V., BOEREFIJN, R., HOUNSLOW, M. J., SALMAN, A. D. & KUIPERS, J. A. M. 2004 Building population balance model for fluidized bed melt granulation: lessons from kinetic theory of granular flow. *Powder Technol.* **142** (2–3), 103–109.

THORNTON, C. & NING, Z. 1998 A theoretical model for the stick/bounce behavior of adhesive, elastic-plastic spheres. *Powder Technol.* **99**, 154–162.

TOMAS, J. R. 2004 Fundamentals of cohesive powder consolidation and flow. *Granul. Matt.* **6** (2–3), 75–86.

VASHISTH, S., AHMADI MOTLAGH, A. H., TEBIANIAN, S., SALCUDEAN, M. & GRACE, J. R. 2015 Comparison of numerical approaches to model FCC particles in gas–solid bubbling fluidized bed. *Chem. Engng Sci.* **134**, 269–286.

VISSER, J. 1989 Van der Waals and other cohesive forces affecting powder fluidization. *Powder Technol.* **58** (1), 1–10.

VAN WACHEM, B. & SASIC, S. 2008 Derivation, simulation and validation of a cohesive particle flow CFD model. *AIChE J.* **54** (1), 9–19.

WANG, J., VAN DER HOEF, M. A. & KUIPERS, J. A. M. 2011 The role of scale resolution versus inter-particle cohesive forces in two-fluid modeling of bubbling fluidization of Geldart A particles. *Chem. Engng Sci.* **66** (18), 4229–4240.

WEBER, M. W., HOFFMAN, D. K. & HRENYA, C. M. 2004 Discrete-particle simulations of cohesive granular flow using a square-well potential. *Granul. Matt.* **6**, 239–354.

https://doi.org/10.1017/jfm.2017.642 Published online by Cambridge University Press